

FINAL
CONTRACT REPORT

**DEVELOPMENT OF AN
EMBEDDABLE MICROINSTRUMENT
FOR CORROSION MONITORING
IN CONCRETE**

ROBERT G. KELLY
School of Engineering and Applied Science
University of Virginia

STEPHEN H. JONES
School of Engineering and Applied Science
University of Virginia



VIRGINIA TRANSPORTATION RESEARCH COUNCIL

FINAL CONTRACT REPORT

**DEVELOPMENT OF AN EMBEDDABLE MICROINSTRUMENT FOR CORROSIVITY
MONITORING IN CONCRETE**

**Robert. G. Kelly, Stephen. H. Jones
School of Engineering and Applied Science
University of Virginia**

(The opinions, findings, and conclusions expressed in this report are those of the authors and not necessarily those of the sponsoring agency.)

Project Monitor

Gerardo Clemeña, Virginia Transportation Research Council
Y. Paul Virmani, Federal Highway Administration

Contract Research Sponsored by
Virginia Transportation Research Council

Virginia Transportation Research Council
(A Cooperative Organization Sponsored Jointly by the
Virginia Department of Transportation and
the University of Virginia)

Charlottesville, Virginia

July 1999
VTRC 00-CR1

NOTICE

The project that is the subject of this report was done under contract for the Virginia Department of Transportation, Virginia Transportation Research Council. The opinions and conclusions expressed or implied are those of the contractors, and, although they have been accepted as appropriate by the project monitors, they are not necessarily those of the Virginia Transportation Research Council or the Virginia Department of Transportation.

Each contract report is peer reviewed and accepted for publication by Research Council staff with expertise in related technical areas. Final editing and proofreading of the report are performed by the contractor.

Copyright 1999 by the Virginia Department of Transportation.

ABSTRACT

The aim of this program was the development of a small and completely embeddable microinstrument for corrosivity measurement in concrete. It should contain all the electronics for the electrochemical measurements, the means for data transfer between engineer and device, and sensors sensitive to the different corrosivity parameters. The goals of the work reported here were to develop and test the required sensors and electronics in a laboratory setting.

Sensors for the measurement of corrosion rate, corrosion potential, chloride concentration, and concrete conductivity were developed and tested in laboratory-scale concrete slabs. The tests included electrochemical chloride driving as a method for test acceleration and wet/dry cycling. The corrosion sensor consists of a piece of reinforcing steel as working electrode, another rebar piece or a platinized Nb-mesh as counterelectrode, and an Ag/AgCl electrode as reference electrode. The conductivity sensor is based on a modified Wenner four-pin method and made of four parallel Au wires. Both sensors work very well. Chloride introduced into the concrete electrochemically induced corrosion on the corrosion sensor, as seen by a decrease in potential and in the polarization resistance. The potentials recovered after more than 1000 h of electrochemical chloride removal, but the corrosion resistance did not regain its original value. The change in chloride content was monitored by a silver/silver chloride chloride sensor. The only present drawback of the microinstrument is the construction of a long-term reliable reference electrode. The best candidates seem to be Ni/W galvanic couple and lead.

A micropotentiostat coupled to a zero-resistance ammeter and a microgalvanostat based on operational amplifiers were designed, and the concepts tested with dummy cells and on carbon steel samples in chloride solutions. The circuits were implemented in different generations of application specific integrated circuits (ASIC), which were successfully tested. The last generation is the heart of a complete measurement system, which includes on two double surface mount boards the ASIC, a microprocessor, control circuitry, and connections to the external corrosivity sensors, as well as RF transceiver circuitry for the wireless communication with the instrument.

FINAL CONTRACT REPORT

DEVELOPMENT OF AN EMBEDDABLE MICROINSTRUMENT FOR CORROSIVITY MONITORING IN CONCRETE

R. G. Kelly, S. H. Jones
School of Engineering and Applied Science
University of Virginia

INTRODUCTION

The degradation of the reinforced concrete infrastructure of the United States represents a monumental cost in terms of unscheduled maintenance and repair as well as a potential public safety concern. This degradation is expected to become increasingly important as the infrastructure continues to age.

Concrete generally provides an environment of very low corrosivity toward steel. The alkaline environment (with low concentrations of aggressive species such as Cl^-) allows the formation of an oxide film that protects the steel. Corrosion rates (proportional to corrosion currents, i_{corr}) are typically low when the concrete is wet and virtually nil when the concrete is dry.¹ Under these conditions, the corrosion potential (E_{corr}) of steel in concrete is high (more positive), in the range of -0.1 V(SCE). The electrochemical behavior of steel in such an environment is shown schematically in Figure 1, line a.

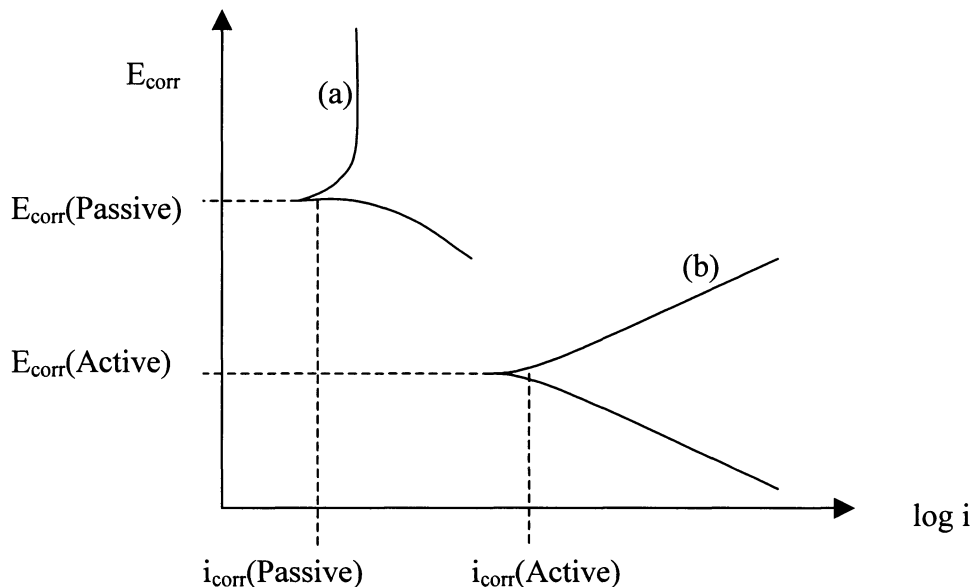


Figure 1. Schematic polarization behavior of steel in concrete in the absence of aggressive conditions (a), and after aggressive conditions have developed (b).

During service, the environment near the steel/concrete interface can become increasingly corrosive due to the ingress of aggressive species such as chloride from deicing salts and/or the

carbonation of the concrete via reaction with atmospheric CO_2 .² As the environment becomes increasingly aggressive, the corrosion rate of the steel increases, which leads to a decrease in E_{corr} . When a critical environment is attained near the steel/concrete interface (often characterized as threshold chloride concentration), the passive film of the steel irreversibly fails, leading to steel corrosion.¹ With the increase in corrosion rate, the E_{corr} drops to more negative values, as shown in Figure 1, line b.

The amount of rebar thickness loss due to the corrosion can be structurally significant. The corrosion products that form have two additional deleterious effects: (1) they degrade the concrete/steel interface, disrupting the load transfer between the two components, and (2) they place the surrounding concrete in tension due to their higher specific volume relative to the steel from which they originate. The latter effect can lead to cracking and increased access to the steel by aggressive species and, therefore, increased corrosion. Both of these effects lead to degradation of the structural strength of the construction (i.e., a bridge).

Current technology for the monitoring of concrete corrosivity relies upon correlation among chemical parameters such as chloride concentration, half-cell potential, and corrosion rate of the reinforcing steel mats. Destructive sampling, potential surveys,³ and electrochemical measurements with reference electrodes or probes embedded in the concrete⁴ are used to examine the corrosion situation of the embedded steel inside concrete. Potential surveys can locate areas of active corrosion by sensing the decrease in open circuit potential that occurs when steel begins to corrode in concrete at an appreciable rate. However, these potential survey results cannot be converted into maps of corrosion *rate* without additional information concerning the electrochemical parameters of the steel, their spatial variation, and a full galvanic corrosion analysis of the entire reinforcing mat. In addition, such potential surveys are only snapshots in time and are generally coarse with respect to spatial variations. Embedded, commercially available corrosion measuring probes offer direct measurements of corrosivity of the concrete to which they are exposed. However, the concrete to which they are exposed may not be directly related to the concrete composition adjacent to the reinforcing steel. In addition, the polarization measurements require highly-trained users in order to take into account the effects of uncompensated ohmic potential drop.⁵ As with the potential survey, electrochemical probes provide snapshots in time and severely limited spatial resolution. Direct electrochemical measurements of the reinforcing mat have been attempted.⁶ However, the complexity of deconvolution of the responses of the various portions of the mat makes this approach untenable for widespread practice.

Thus, there exists a need to develop a corrosivity measurement system that can be contained within the concrete and provide direct measurements of the corrosivity of the environment to act as an early warning system that has information concerning the spatial distribution of the corrosivity. A complete measurement system should be capable of making accurate measurements of corrosion rate (*e.g.*, polarization resistance) but also simultaneously other important parameters (*e.g.*, temperature, chloride ion concentration, and conductivity). The engineer could then use all this information to assess the situation and make a fully informed decision concerning which mitigation strategies, if any, to apply.

PURPOSE AND SCOPE

The purpose of this study was to develop a completely embeddable microinstrument for corrosivity measurement in concrete. The study required the design of the electronics and the implementation and adaption of suitable sensor concepts for the different corrosivity parameters.

The corrosion measurement system (Figure 2) was conceived with the following components:

1. several sensors (*e.g.*, for electrochemical measurements of corrosion rate, pH, temperature, chloride ion concentration, conductivity)
2. a potentiostat with an autoranging zero resistance ammeter (ZRA) for electrochemical measurements
3. high input impedance amplifiers for the various sensors
4. analog-to-digital (A/D) and digital-to-analog (D/A) converters
5. a microprocessor capable of controlling the electrochemical measurements, managing the measurements from the sensors, integrating the information from the various sensors
6. a means of communicating externally via either a serial communications port or microwave telemetry
7. a reliable power source.

Such individual systems are commercially available. However, these systems are cumbersome and are unsuitable for embedding in the concrete on a larger scale.

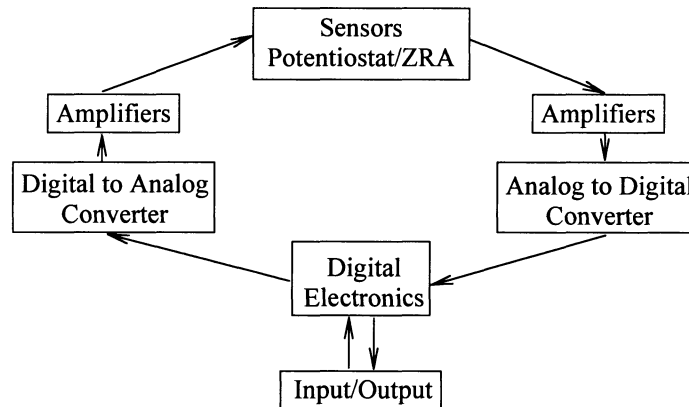


Figure 2. Design of embeddable microinstrument for corrosivity measurement.

Commercially available systems made of large, discrete instruments are not well suited to the introduction of a large network of independent corrosion monitoring systems. If the measuring device (*e.g.*, a data logger or computer) is connected at an external site to tethering cables that emerge from the structure, monitoring of corrosive conditions in aggressive environments (rain, deicing salts, seawater) is difficult. At the location where the cables leave the concrete, water and chloride ingress into the structure could be enhanced. Reinforced concrete or off-shore structures are two examples where the environments limit the system reliability for such arrangements. Therefore, it would be advantageous if the entire microsystem, including all the electronics and data transmission, was embeddable.

Our approach to the design of the concrete corrosivity microinstrument followed a set of key tenets:

1. It is more practical to know corrosivity rather than the corrosion rate of a portion of actual structure.
2. Increase the reliability of the overall assessment by coupling several different types of measurements related to corrosivity.
3. Design circuits to be sufficient for the task in order to minimize power consumption. For example, most data processing should be done outside the device.
4. The heart of the system, an application-specific integrated circuit (ASIC) would perform only those functions that are not commercially available on other chips but would be flexible enough to easily perform a range of measurements. In this way, we take advantage of what is commercially available but also provide an ASIC that is an enabler for other electrochemical and corrosion monitoring applications.
5. Make the microinstrument sufficiently small and inexpensive to allow networks of systems to be deployed cost effectively.
6. Deploy a wireless system that is embeddable in the structure during construction or repair; neither communications nor power should require hardwire connections from the device to the outside.
7. Make the system durable to allow monitoring processes to be followed over structural lifetimes.
8. Seek to transfer the developed technology as soon as possible for commercial manufacture of the microinstrument.

METHODS AND MATERIALS

Electrochemical Measurements in Concrete

By monitoring the corrosion potential of steel in concrete, the corrosion activity of the steel can be assessed. Such a measurement is fairly straightforward and is the basis for the potential surveys routinely made as all that is required is an electrical connection to the rebar and a reference electrode that is placed in reasonable proximity to the steel (for example, on top of the concrete). Unfortunately, interpretation of such measurements can be difficult, and no rate information is extractable. Corrosion rate measurement can be accomplished using polarization resistance measurements.⁶ In theory, these measurements can also be made remotely, but many complications in interpretation exist when the reinforcing structure has a spatial distribution of active and passive regions, as is usually the case. Measured chloride concentrations in concrete are not direct measurements of corrosivity, and often the very nature of the sampling is intrusive. Nonetheless, these parameters (corrosion rate, E_{corr} , chloride concentration ($[Cl^-]$)) can be used together to assess the corrosivity of a region in concrete if they are measured simultaneously. Additional parameters, such as conductivity and temperature, can provide supplementary information that can be used to enhance the reliability of any corrosivity measurement.

Three of the corrosivity parameters (E_{corr} , i_{corr} , and $[\text{Cl}^-]$) are electrochemically measurable, using very similar circuitry involving an operational amplifier (OPAMP) as the basic building block. A buffer amplifier provides a high impedance interface to measure voltages without affecting the interfaces under study. Measurements of E_{corr} , conductivity, and $[\text{Cl}^-]$ require such a measurement. The E_{corr} measurement compares the voltage of the steel working electrode to that of a reference electrode. The $[\text{Cl}^-]$ can be quantitatively assessed by comparing the voltage of a Ag/AgCl ion specific electrode (ISE) to that of a reference electrode. Figure 3 shows schematics of the two other circuits required. Figure 3a shows a galvanostat (μGstat), which when coupled with the buffer amplifier allows conductivity measurements to be made. Figure 3b shows a potentiostat (μPstat) and a zero resistance ammeter (μZRA) as well as a dummy cell used to test the circuitry. These devices are required for the polarization resistance measurements and many other electrochemical measurements.

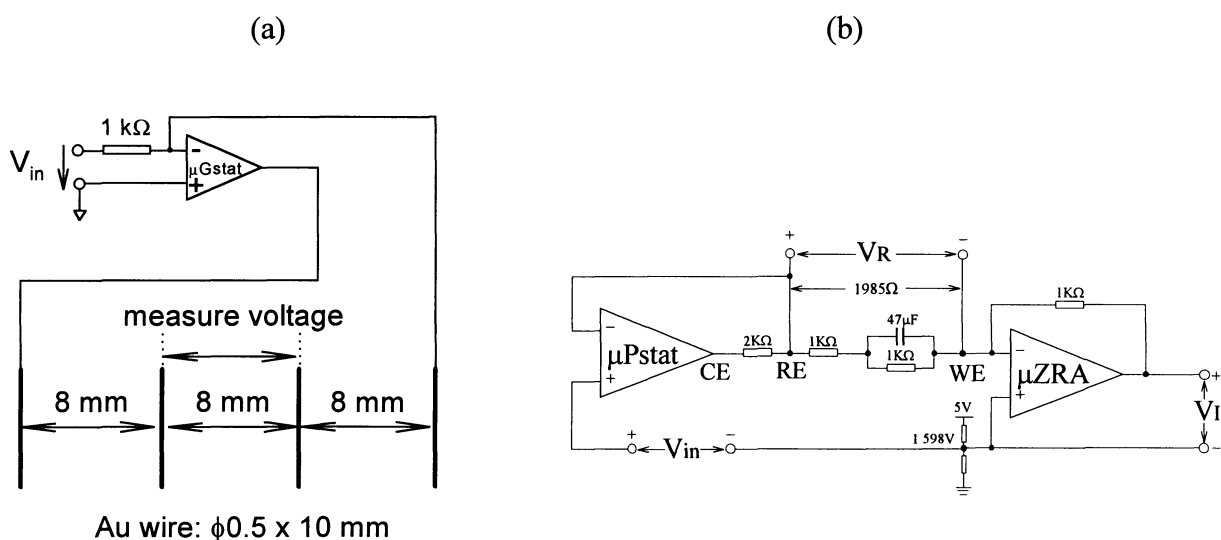


Figure 3. Schematics of (a) conductivity measurement and (b) polarization resistance circuits.

Our initial work focused on the design and implementation of the required electrochemical measurement circuits into an application specific integrated circuit (ASIC). The electrical circuit work took advantage of the national infrastructure that has accompanied the explosion in microelectronics applications.

The Metal Oxide Semiconductor Implementation Service (MOSIS) acts as a clearinghouse that accepts computer-aided designs of integrated circuits and implements them through the very large scale integration (VLSI) manufacturing process for U.S. universities and small businesses. All of the components discussed in the present work were designed according to the rules implemented by MOSIS for its $2.0\ \mu\text{m}$, double polysilicon, analog/digital complementary metal oxide semiconductor (CMOS) process and the $1.2\ \mu\text{m}$ CMOS process, respectively.

A complete, wireless microinstrument requires not only the measurement electronics described, but also a microprocessor, control circuitry, digital-to-analog and analog-to-digital converters, and communication circuitry. The microprocessor is required to manage the

measurements and the communication with the outside. A multiplexer allows the same measurement circuits to be used for a variety of purposes (*e.g.*, measurement of E_{corr} and $[\text{Cl}^-]$). This reduces the power needs of the microinstrument. The wireless communication circuitry is required to allow the device to be controlled from the outside without tethering.

Circuit Testing Procedures

Each of the components was tested individually to determine performance characteristics using conventional electrical characterization methods, details of which are available elsewhere.⁷ The micropotentiostat/ZRA combination was tested as a stand-alone device using the configuration shown in Figure 3b. Stepwise, potentiostatic polarization resistance measurements were made (5 mV or 100 mV steps, 30 s step time) on off-chip dummy cells and actual corroding systems. The dummy cell studied was a combination of a 1 k Ω resistor in parallel with a 47 μF capacitor, with this parallel combination in series with a 1 k Ω and a 2 k Ω resistor as also shown in Figure 3b. All resistors had a 1% tolerance.

Polarization resistance measurements were conducted on carbon steel samples (4.9 cm²) immersed in 0.6 M NaCl, saturated Ca(OH)₂, or saturated Ca(OH)₂ + 0.6 M NaCl solutions in the same manner as with the dummy cell. The polarization resistance value was calculated from the resulting current/voltage curves via linear regression. The results from the micropotentiostat were compared to results from commercially available electrochemical corrosion measurement systems.

In the first generation design, standard electrochemical electrodes were used in testing. These had exposed areas on the order of several square centimeters, and all testing was performed in aqueous solutions. In the second generation of testing, miniature probes for polarization resistance, conductivity, temperature, and pH were designed and tested in both aqueous solution and concrete. This testing was performed with both operational amplifiers, integrated into a single ASIC, and commercial instruments for comparison.

Miniature Sensor Concepts

The microsensors were developed to monitor corrosion rate and changes in resistivity, chloride concentration, and pH in concrete. The corrosion sensor was composed of two pure iron strips (working and counter electrodes) and a Ag/Pb galvanic couple⁸ or Ag/AgCl electrode (reference electrode) as shown in Figure 4. The two iron strips, separated by 5 mm, were placed on the same plane. The reference electrode was located between the two strips. In later sensor designs, the pure iron strips were replaced with rebar strips.

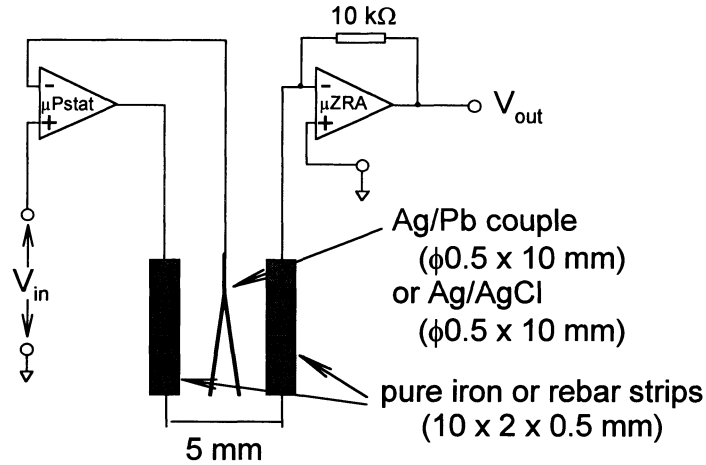


Figure 4. Schematic of corrosion (R_p) sensor with steel working and counter electrodes and either a Ag/Pb or Ag/AgCl reference electrode.

The resistivity of concrete was measured using a modified Wenner four-pin electrode method. Four gold electrodes ($\phi 0.5 \times 10$ mm) were placed on the same plane with an equal separation of 8 mm as shown in Figure 3a. The principle of this method of resistivity measurement is to apply a constant current between two outer electrodes and then record the potential drop across two inner electrodes. The calculated resistance between two inner electrodes is thus converted to resistivity according to the following equation:

$$\rho(\Omega \cdot \text{cm}) = 2\pi aR = (SC)R \quad [1]$$

where a is the electrode separation, R is the resistance, and SC is the sensor constant. Because the resistivity sensor developed in this work is different from that used in the standard method,⁹ it was calibrated in NaCl solutions of known resistivity to determine the sensor constant before being embedded in concrete. The configuration of an operational amplifier to form a microgalvanostat (μGstat) for the measurement of concrete resistivity is shown in Figure 3a.

Ag/AgCl electrodes were used to detect chloride in concrete. They were made from pure Ag wires ($\phi 0.5 \times 10$ mm) in 0.1 M HCl by applying a oxidizing current of 0.4 mA/cm^2 for 30 min. The calibration curves for chloride sensors were made in saturated $\text{Ca(OH)}_2 + \text{Cl}^-$ solutions. The pH sensors tested in this work involved two types: W/WO_3 ¹⁰ and IrO_2 .¹¹ W/WO_3 electrodes were made by immersing pure W wires ($\phi 0.5 \times 10$ mm) in 0.1 M HNO_3 for 72 h while the Ir/IrO₂ electrodes were prepared by cyclic voltammetric treatment of pure Ir ($\phi 0.25 \times 10$ mm) in 0.5 M H_2SO_4 at a scan rate of 50 to 1000 mV/s for 3.5 to 10 h. Both types of pH sensors were calibrated in buffer solutions and NaCl + Ca(OH)_2 solutions.

Several metals, oxides, and metal A/metal B galvanic couples were tested to determine if they could be used as a long-term stable reference electrode in concrete.

Concrete Test Structures

The first test structure was designed for the preliminary evaluation of the $\mu\text{Pstat}/\mu\text{ZRA}$ combination and microsensors (Figure 5). A commercial LMC 6034 OPAMP chip was used to form a Gstat configured as in Figure 3a. The concrete contained 2548 g Type II cement, 6507 g coarse aggregate (ϕ 6.5 to 9.5 mm), 2503 g fine aggregate (through No. 4 mesh), and 1274 g tap water, which was cast into a slab of $200 \times 200 \times 100$ mm. The slab cured for 18 days in a moisture room. This concrete slab contained one sensor assembly (corrosion sensor, resistivity sensor, pH, and chloride electrodes placed on an acrylic plate and connected directly to a $\mu\text{Pstat}/\mu\text{ZRA}$ configured by the OPAMPs on a LMC 6034 OPAMP chip) and a corrosion sensor connected to the commercial electrochemical measuring system. Also embedded in the concrete slab were an ERE 20 commercial reference electrode ($\text{MnO}/\text{Mn}_2\text{O}_3$) and a rebar specimen (ϕ 12 mm) to allow comparison of the corrosion rate to the pure iron.

The potentials of sensors and electrodes were recorded versus the $\text{MnO}/\text{Mn}_2\text{O}_3$ electrode, which in turn was monitored by a saturated calomel electrode immersed in the testing solution. All potentials reported in the results are on the SCE scale. All these sensors and electrodes were placed at the same level 10 mm from the concrete surface to be exposed to the testing solution. A second platinized Ti mesh (approximately 150×150 mm) was placed 60 mm above the immersion surface in the immersion solution to assist in the electrochemical intrusion of chloride ions. All concrete surfaces except that in contact with the solution were sealed with Armstrong epoxy. After the concrete slab was exposed to 0.6 M NaCl for about 150 h, which allowed the stabilization of sensors and electrodes, a constant current of 25 mA was applied to the two platinized meshes inside and outside of the concrete slab with the Ti-mesh in concrete acting as the anode. Because of their negative charge, Cl^- ions migrate into concrete under this electrical field. It was quickly determined that the concrete block needed to be oriented as shown in Fig. 5 to allow the escape of bubbles generated at the auxiliary Ti mesh during the Cl^- driving.

The objectives of having the second test structure (concrete block, $200 \times 200 \times 100$ mm, Figure 6) were to test a different pH sensor as well as the first iteration of the ASIC. In the second test structure, two OPAMP chips of the second VLSI design were used for the $\mu\text{Pstat}/\mu\text{ZRA}$ combination and μGstat . To ensure a uniform distribution of Cl^- over the cross-section inside the concrete slab during Cl^- intrusion, coarse aggregate was not used and the mortar compositions were 2548 g Type II cement, 7371 g fine aggregate (through No. 4 mesh), and 865 g deionized water. The microsensor designs were identical with those in the first test structure except that rebar material was used for the working and counter electrodes in the corrosion sensors and the W/WO_3 pH sensors were replaced by Ir/IrO_2 electrodes. The microsensors were located at four different distances from the wetted surface of concrete. At level 1, two sensor assemblies were embedded, each of which had one corrosion sensor, one resistivity sensor, one Ag/AgCl electrode, and two Ir/IrO_2 electrodes. Two rebar specimens (1 cm^2) and a commercial ISFET (Ion selective field effect transistor) pH electrode were also placed on this level for the comparison of corrosion rate and pH. The sensor assemblies at levels 2 and 3 contained one corrosion sensor, one Ag/AgCl , and Ir/IrO_2 electrodes. Level 4 was outside the electrical field, and Cl^- was not expected to migrate into this region in the electrochemical intrusion process. The sensor assembly at level 4 had one more Ir/IrO_2 electrode

than those at levels 2 and 3. In addition, a temperature sensor was embedded at a position close to level 4.

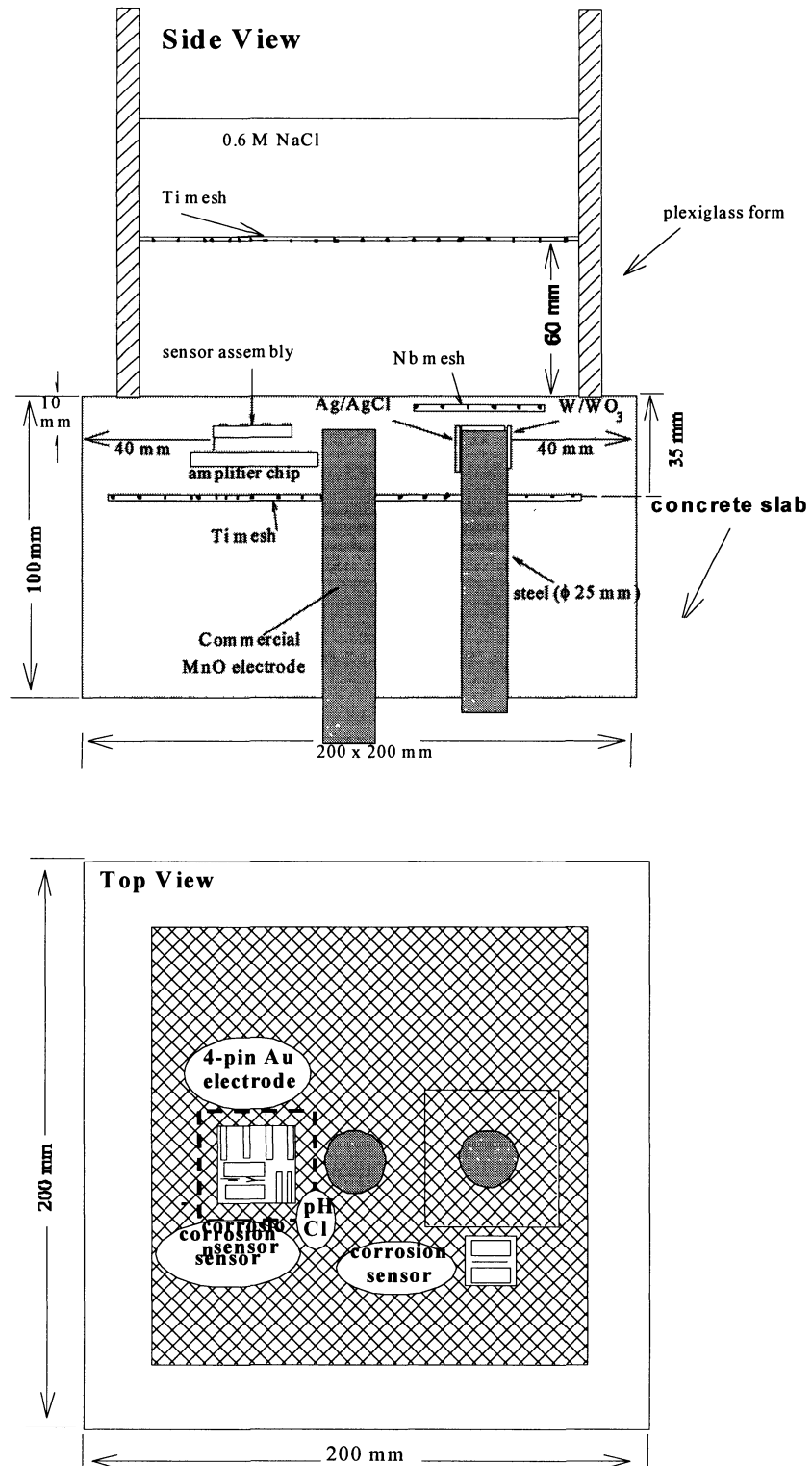


Figure 5. Schematic side and top views of assembly embedded in Concrete Test Structure 1.

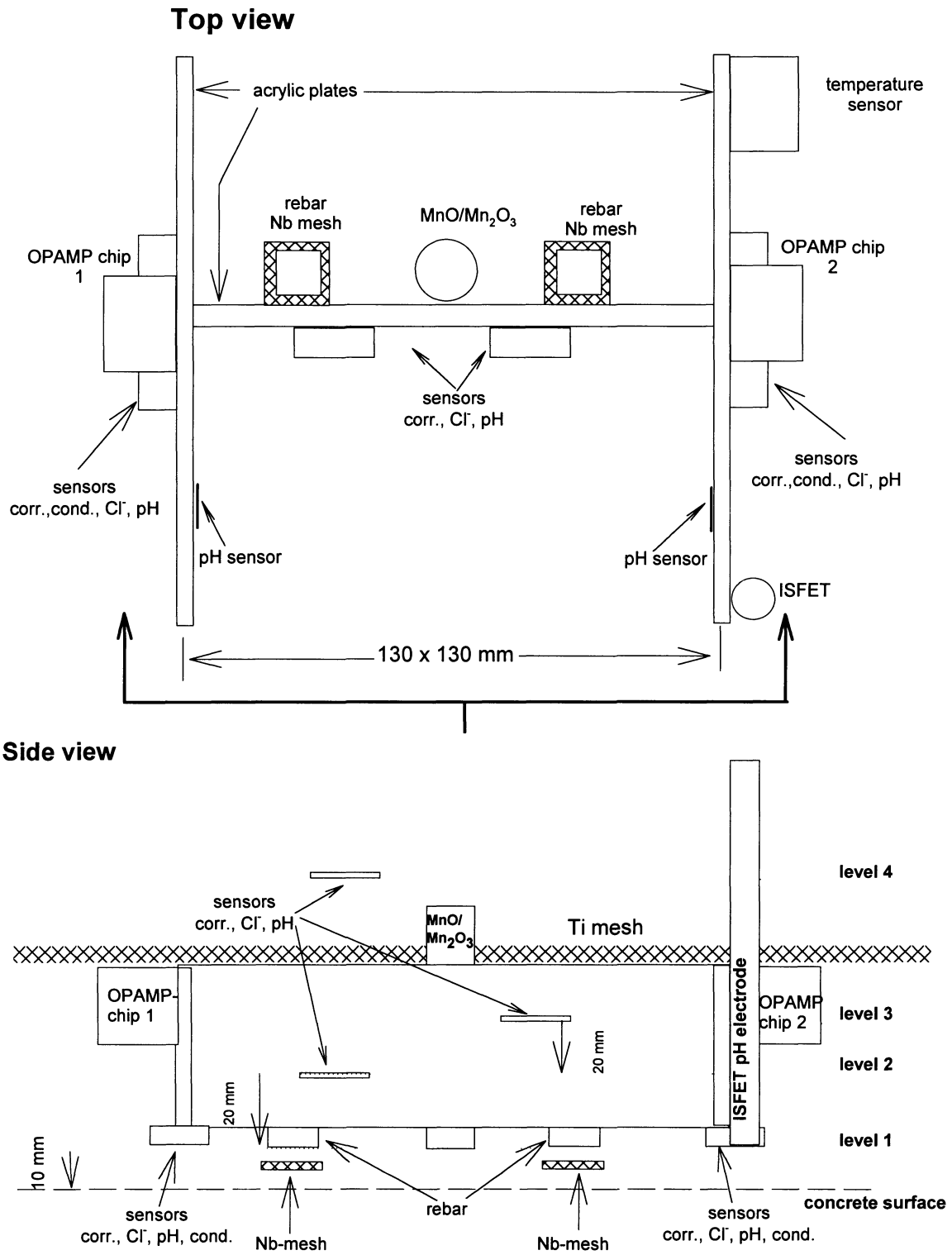


Figure 6. Concrete test structure 2 showing structures that held sensors and other electrodes.

A third test structure was used to create a set of concrete slabs with a range of chloride contents. These slabs were made from 865 g cement (Type II), 2184 g coarse aggregate (ϕ 6.5 to 9.5 mm), 819 g fine aggregate (sand, through No. 4 mesh), 423 g water, and NaCl: 0 to 0.2 wt. % of the concrete. After production, these slabs were allowed to cure in a moisture room for 14 days.

The objectives for this test structure were: (1) calibration of the Cl^- sensor (Ag/AgCl) in concrete, (2) calibration of resistivity sensor against moisture content, (3) testing of different reference electrode materials, and (4) testing of candidate coating materials to be used in sealing of feedthroughs in the microinstrument. Each slab used the test structure design shown in Figure 7.

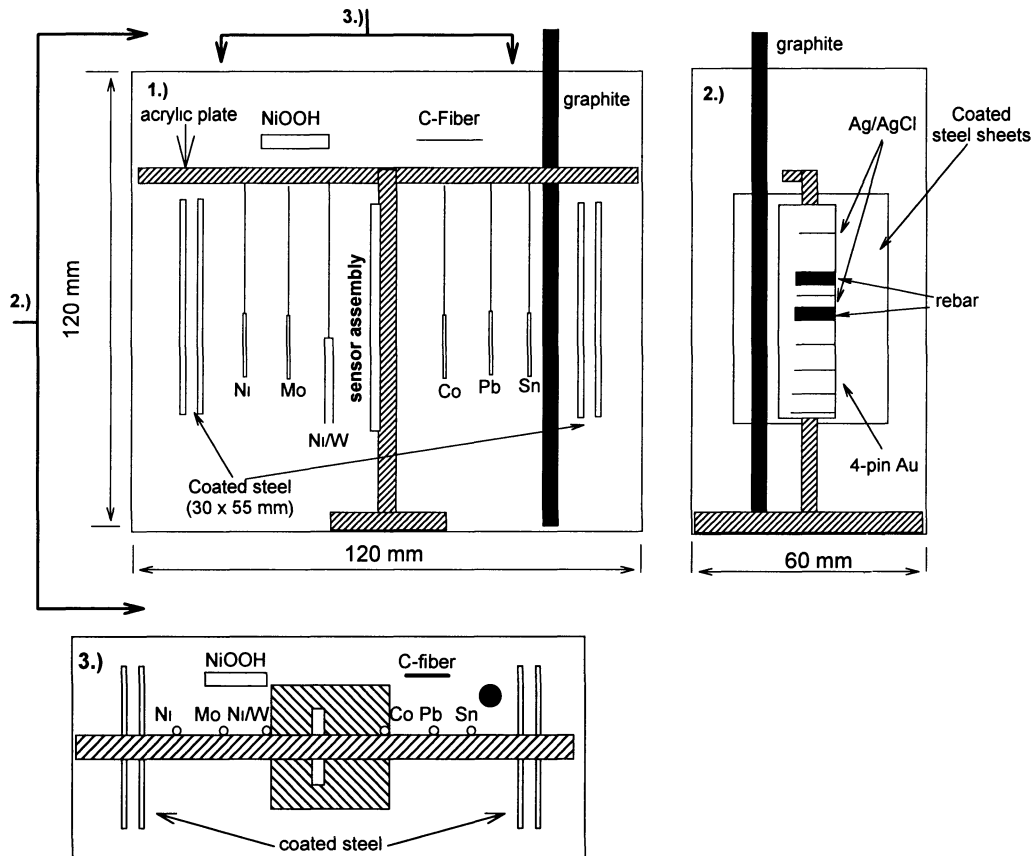


Figure 7. Design of test structure 3.

Embedded within each slab were a sensor assembly (one corrosion sensor (see Fig. 4), one resistivity sensor, and two Ag/AgCl sensors), reference electrodes (wires of Ni, Mo, Co, Pb, Sn, NiOOH, C-fiber, Ni/W, and graphite), and four carbon steel sheets (30×55 mm), each with a different kind of coating. Table 1 gives a description of the content of each slab in the set.

Table 1. Sensors and materials embedded in slabs from Test Structure 3. (cmp. fig. 7).

Material	Slab 1	Slab 2	Slab 3	Slab 4	Slab 5	Slab 6	Slab 7
Corrosion sensor	✓	✓	✓	✓	✓	✓	✓
Resistivity (4-pin)	✓	✓	✓	✓	✓	✓	✓
Ag/AgCl (Cl ⁻ sensor)	✓	✓	✓	✓	✓	✓	✓
Ni/W couple	✓		✓		✓		
Co	✓		✓		✓		✓
Ni	✓		✓		✓		✓
Mo	✓		✓		✓		✓
Pb	✓		✓		✓		✓
Sn	✓		✓		✓		✓
NiOOH	✓		✓		✓		✓
graphite	✓		✓		✓		
C-fiber	✓		✓		✓		✓
E-bond (60/100 μm)	✓		✓		✓		
Amstrong(60/100 μm)	✓		✓		✓		
Interlux (60/100 μm)	✓		✓		✓		
Polibrid 680/705 (60/100 μm)	✓		✓		✓		
Cl ⁻ (weight % in concrete)	0.00	0.005	0.010	0.020	0.050	0.100	0.200

After removal from the moisture room, the slabs were treated as follows:

1. All seven slabs were first immersed in saturated Ca(OH)₂ for 18 days to attain steady state for all the sensors and electrodes.
2. The slabs were removed from the saturated Ca(OH)₂ solutions and placed in a moisture chamber. The relative humidity was decreased in the order 90, 70, 50, and 30%. Each humidity level was kept constant for one day.
3. Slabs 1, 3, 5, 6, and 7 were then dried in air (30 to 50%RH), whereas slab 2 was heated at 105 C for two days and slab 4 at 60 C for 1 day and then dried in air. The heating was

performed to remove the humidity in the slabs more efficiently. After heating, some large cracks were found on the surface of slab 2 and some fine cracks on the surface of slab 4. The total time of drying was about 2000 h for all slabs.

4. After the drying, all the slabs were immersed in saturated $\text{Ca}(\text{OH})_2$

Chloride was electrochemically driven into slab 3 using the cell arrangement shown in Figure 8. This was done to test the chloride sensor, to investigate if the potential of the reference electrodes responds to changes in the chloride concentration, and to study the breakdown of passivity and repassivation upon chloride intrusion / removal. To remove the Cl^- in the concrete slab, 1 M NaCl was replaced by saturated $\text{Ca}(\text{OH})_2$ and the polarity of the applied current was reversed.

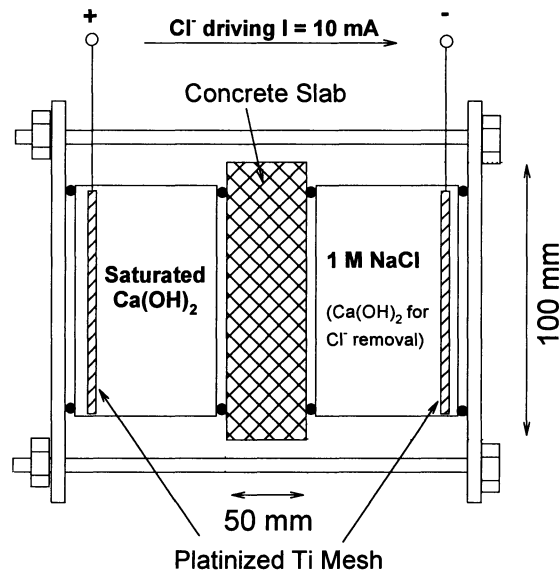


Figure 8. Clamping cell used to perform chloride driving into and out of slab 3 from test structure 3.

RESULTS AND DISCUSSION

Circuit Design and Performance

Initial Design

Two VLSI designs were submitted to MOSIS. Figure 9 shows the first design submitted to MOSIS, which consisted of a 2.2 x 2.2 mm chip containing eight OPAMPS. This chip was used to test the micropotentiostat/zero resistance ammeter concept. Six copies of this chip were returned in 40-pin, dual-inline packages.

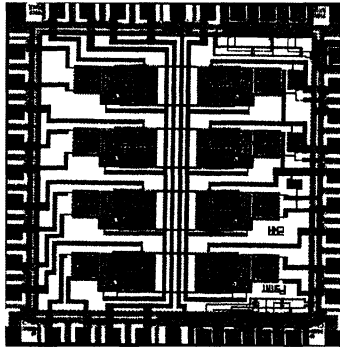


Figure 9. CAD design for 8 operational amplifiers on a 2.2 x 2.2 mm silicon chip.

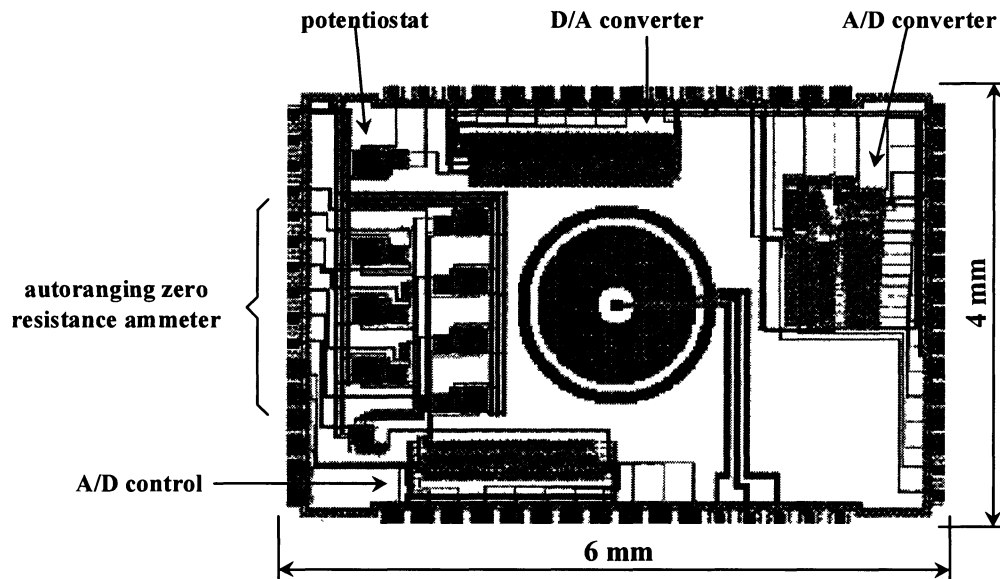
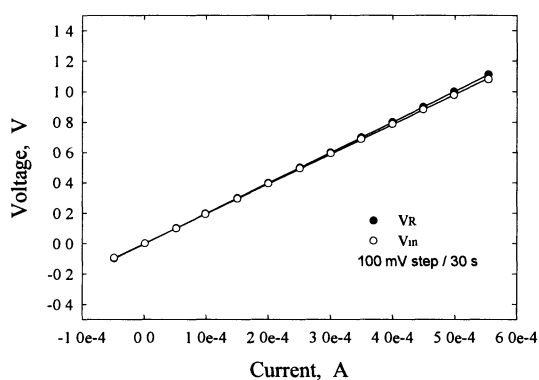


Figure 10. CAD design of first generation ASIC with on-chip electrodes, an autoranging ZRA, and ADC and DAC. Overall dimensions were 4.6 x 6.8 mm.

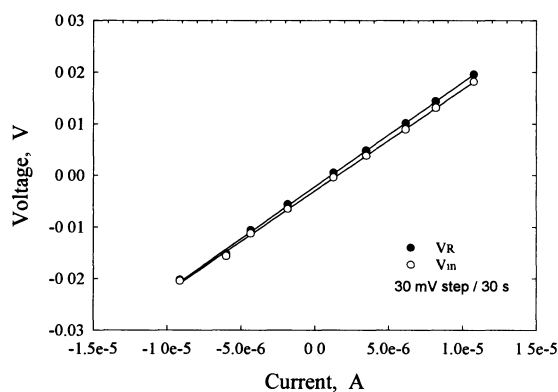
Figure 10 shows the second design submitted to MOSIS, which contained three on-chip electrodes for electrochemical measurements, as well as analog integrated circuits for amplification and signal conditioning, A/D and D/A conversion, and a micropotentiostat with an autoranging ZRA on a 4 x 6 mm chip. The on-chip electrodes, however, were deemed to have reliability issues when we considered access of the concrete pore solution and need for long service life. The latter design was returned in 64-pin, MOSIS-standard packages. This package configuration was chosen in order to facilitate testing of the individual components.

Table 2. Operating characteristics of ORNL (Oak Ridge National Laboratories) operational amplifier using a 5 V power supply.

Characteristic	Condition	Typical
Operating Range		1 to 4 V
Voltage Gain		10,000
Offset Voltage	Unity Gain	± 50 mV
Small Signal Bandwidth	Unity Gain	2 MHz
Slew Rate	3 V Pulse	4 V/ μ s
Full Power Bandwidth	3 V Pulse	425 kHz
Supply Current	10 k Bias Resistor	1.6 mA
Power Consumption	10 k Bias Resistor	8 mW



(a)



(b)

Figure 11. Polarization results for dummy cell using first generation operational amplifiers (Figure 9). (a) Large amplitude polarization, (b) small amplitude polarization.

Table 2 lists some of the basic operating characteristics of the operational amplifiers that comprise the micropotentiostat/ZRA and are used as amplifiers for other sensors as well. Potentiostatic polarization curves developed for the dummy cell are shown in Figure 11. Figure 11a shows the results from a scan from -0.1 V to +1.1 V in 100 mV steps. The two curves represent data using either the voltage V_{in} applied to the input terminals of the micropotentiostat (Figure 3b) or the voltage measured between the WE and RE connections, V_R . For an ideal operational amplifier, V_R would be equal to V_{in} . Excellent linearity was observed between the measured current and both V_{in} and V_R . Regression analyses gave values of 2008 Ω and 1963 Ω for the data using V_R and V_{in} , respectively. These values compare within 1.2% of the actual value of the DC resistance of the dummy cell of 1985 Ω . A small offset was observed between V_{in} and V_R , amounting to 10 mV at an applied voltage of 1 V.

The accuracy of the micropotentiostat for small amplitude measurements such as polarization resistance, was also assessed. Potentiostatic polarization measurements were made on the same dummy cell over ± 20 mV using 5 mV steps as shown in Figure 11b. Linear regression analyses gave values of 2018Ω and 1962Ω using V_R and V_{in} , respectively, which are within 1.7% of the actual value. The correlation coefficient was 0.9992. For comparison, the same experiments were conducted with a commercial corrosion measurement system. The resistance value from these data was 1992Ω , with a correlation coefficient of 1.0. Thus, the microinstrument performed very well even for small amplitude measurements.

Figure 12 shows the results of polarization resistance (R_p) tests on carbon steel exposed to 0.6 M NaCl at room temperature using the micropotentiostat. The microinstrument data generated a value of R_p of $3.42 \text{ k}\Omega\text{-cm}^2$, with a correlation coefficient of 0.999. The potential reported for the microinstrument was that measured between the working and reference electrodes. Using the commonly accepted value of 0.021 V for the B factor in the Stern-Geary relationship yields a corrosion rate of $6 \mu\text{A}/\text{cm}^2$ (2.8 mpy), a quite reasonable value for steel in salt water.^{12,13} For comparison, a commercial potentiostat gave a polarization resistance of $3.13 \text{ k}\Omega\text{-cm}^2$ with a correlation coefficient of 0.971.

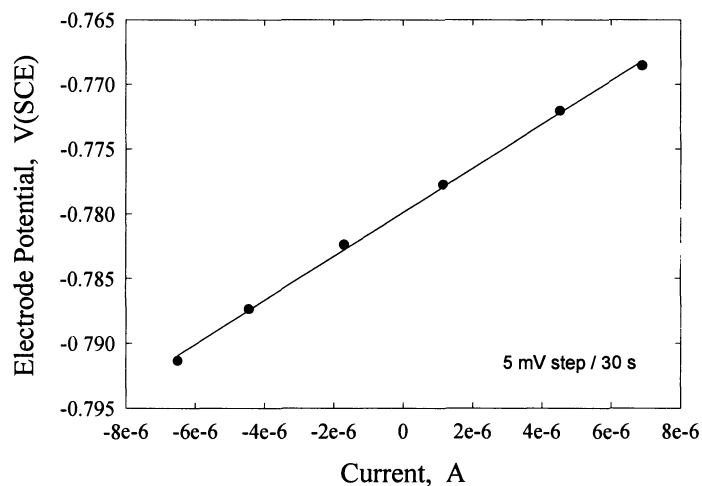


Figure 12. Polarization resistance data of steel in 0.6 M NaCl collected with the first generation operational amplifiers (Figure 9).

The results of the polarization resistance measurements made on steel in saturated $\text{Ca}(\text{OH})_2$ and saturated $\text{Ca}(\text{OH})_2 + 0.6 \text{ M NaCl}$ measured by the microinstrument and by the commercial apparatus are shown in Table 3. Again, excellent agreement in the measurement of R_p between the two measurement systems was obtained: $201 \text{ k}\Omega\text{-cm}^2$ by the micropotentiostat vs. $194 \text{ k}\Omega\text{-cm}^2$ by the commercial system for saturated $\text{Ca}(\text{OH})_2$. These polarization resistances would correspond to a corrosion rate of approximately $0.1 \mu\text{A}/\text{cm}^2$, which is in excellent agreement with that expected for steel in $\text{Ca}(\text{OH})_2$ solution.^{14,15} In the solution of saturated $\text{Ca}(\text{OH})_2 + 0.6 \text{ M NaCl}$, the polarization resistance was much lower, indicating more rapid corrosion. This change was detected by both the micropotentiostat ($R_p = 7.7 \text{ k}\Omega\text{-cm}^2$) and the commercial system ($R_p = 8.8 \text{ k}\Omega\text{-cm}^2$). It should be noted that the measurement was made first with the commercial instrument, indicating that the corrosion rate was increasing with time, as would be

expected. These results demonstrate that the microinstrument is capable of measuring corrosion rates over a wide dynamic range.

Table 3. Polarization resistances of steel measured with a commercial system and the micropotentiostat.

Solution Composition	Measured Polarization Resistance(kΩ -cm ²)	
	Commercial System	Micropotentiostat
Saturated Ca(OH) ₂	194	201
Saturated Ca(OH) ₂ + 0.6 M NaCl	8.8	7.7

This phase of the work demonstrated the viability of producing the components necessary for a microsystem capable of making electrochemical measurement of corrosion rate using VLSI circuit design and manufacturing.

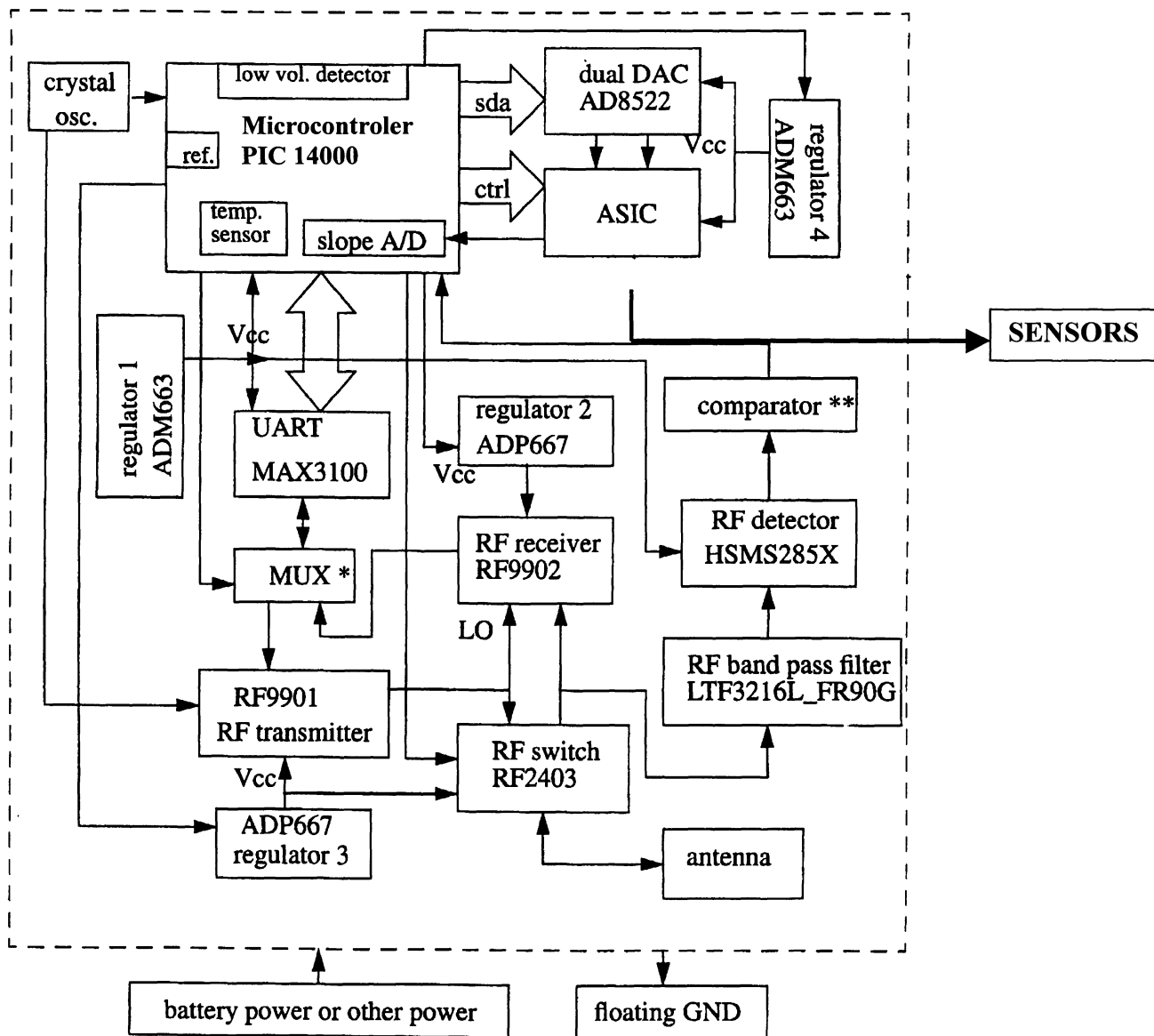
Final Design and Implementation of System Microelectronics

During the last phase of the project, our efforts have been focused in the following areas:

1. completion of the design and fabrication of the system microelectronics for measurement of corrosivity, including programming of the microprocessor
2. design and implementation of the two surface mount boards that will contain the microelectronics
3. testing of prototype assembled on testing board
4. testing of wireless communication circuitry
5. testing of packaging schemes for microsystem.

An expanded high-level design of the microsystem electronics is shown in Figure 13. All testing results have shown that the electronics performance is fully sufficient for all types of measurements associated with the corrosivity monitoring. However, there have been numerous engineering modifications at the software and hardware level during recent testing, analysis, and review of our prototype system.

System Block Diagram



Note: * Digital MUX included in ASIC
 ** Comparator included in PIC14000

Figure 13. System block diagram of a microinstrument.

A complete working prototype was fabricated on a large prototype board in order to program the microprocessor and test the complete system. The prototype includes the front-end ASIC for corrosivity measurements, the microprocessor and associated circuitry, as well as off-the-shelf RF communication circuits. In this way, all the firmware and software for the system was fully developed and is presently functioning. There were substantial challenges associated with including the entire system functionality into the limited memory and program space of the microprocessor, but at this time all the functionality in the proposed high-level design has been

included. We have also focused on experimentally evaluating the front-end corrosivity ASIC with regard to leakage current and offset voltage (25 mV in μ Pstat and 15 mV in μ ZRA). As expected, the performance is not quite as good as off-the-shelf, discrete components (maximum current capacity 1 mA instead of 2 mA, reduced linear range, current leakage, larger offset voltages), but the performance is acceptable for polarization resistance monitoring, chloride sensing, and conductivity sensing in this application. Several modifications were made to the RF front end circuitry to include an additional encoding and decoding step to improve data transmission and reception reliability. After verifying the operation of the prototype system on a testing board, the design and implementation of the two surface mount boards that will contain all the electronics in the final device was initiated. The first double-sided surface mount board was designed and implemented; this board (known as the Eboard) contains the microprocessor, control circuitry, and connections to the external corrosivity sensors. The board is working but still under evaluation for reliability. The second board, containing the RF transceiver circuitry (known as the Rfboard) has been fabricated and tested successfully.

The results of initial testing of commercial RF transmission circuits were highly encouraging, with microwaves at 915 MHz and 896 MHz being detected through 12.5 cm of concrete (both wet and dry) despite the use of a non-optimized antennae for transmission.

The Eboard has been connected to the prototype RF transceiver board, dummy cells, and real electrochemical cells. Complete system functionality has been tested. This testing included (1) remote transmitter RF prompt and command query of the embeddable microinstrument, (2) system measurement of polarization resistance, conductivity, temperature, and chloride content, and (3) transmission of the microinstrument results approximately 15 m to a remote receiver.

Examples of the performance are shown in Figures 14 through 16. The prototype device was used to measure the polarization resistance of the rebar working electrode in saturated $\text{Ca}(\text{OH})_2$ and saturated $\text{Ca}(\text{OH})_2 + 0.6 \text{ M NaCl}$. In both cases the agreement with a commercial measurement system was excellent (Figure 14).

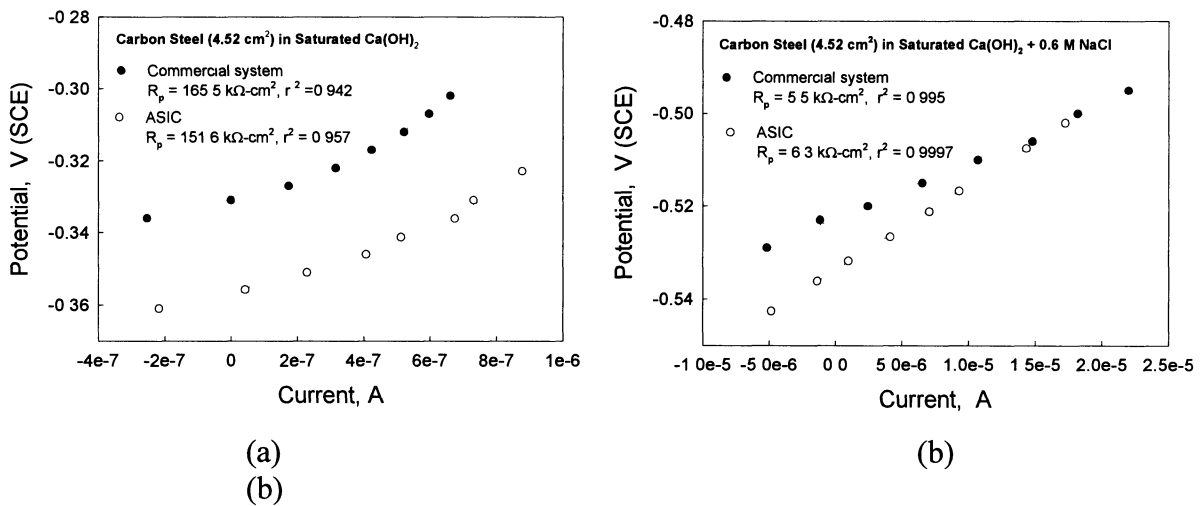


Figure 14. Comparison of polarization resistance measurements from prototype microsystem with a commercial system on steel in (a) saturated $\text{Ca}(\text{OH})_2$, and (b) saturated $\text{Ca}(\text{OH})_2 + 0.6 \text{ M NaCl}$.

Figure 15 shows the performance of the prototype microinstrument in the measurement of polarization resistance and open circuit potential for sensors embedded in test structure 2. This slab had been dried in air for more than 4 months after all measurements. After re-immersion in 0.6M NaCl for 3 days, the E_{corr} and polarization resistance of the corrosion sensors embedded near the surface (level 1, see Figure 6) were still in the active state. With increasing distance from the concrete surface (levels 2 and 3), the E_{oc} increased, indicating a transition from the active state to a passive state. Agreement with the commercial measurement system was also excellent in this case.

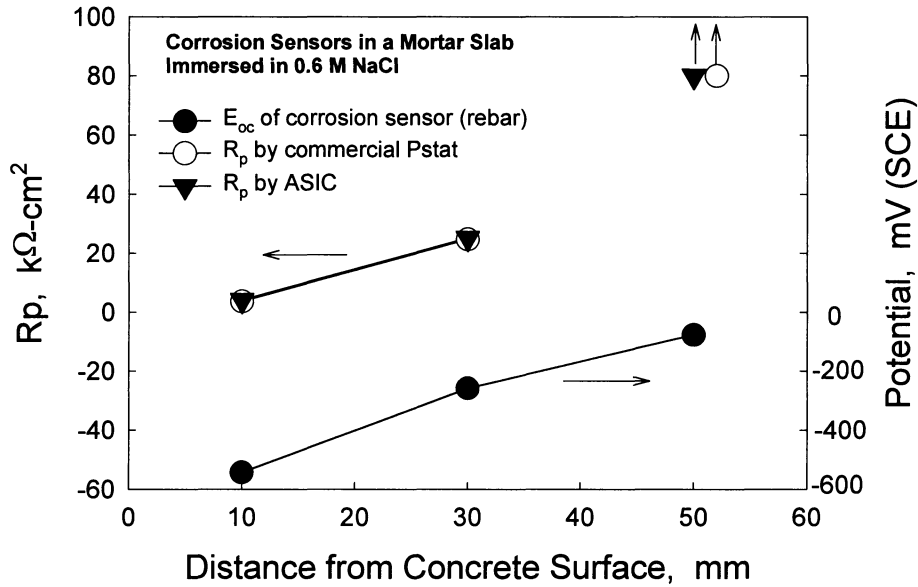


Figure 15. Open circuit potential and polarization resistance measurements on corrosion sensors embedded in mortar slab using prototype microinstrument (ASIC) and commercial potentiostat. Note that at the 10 and 30 mm distances, the R_p measured by the commercial system and the ASIC is identical.

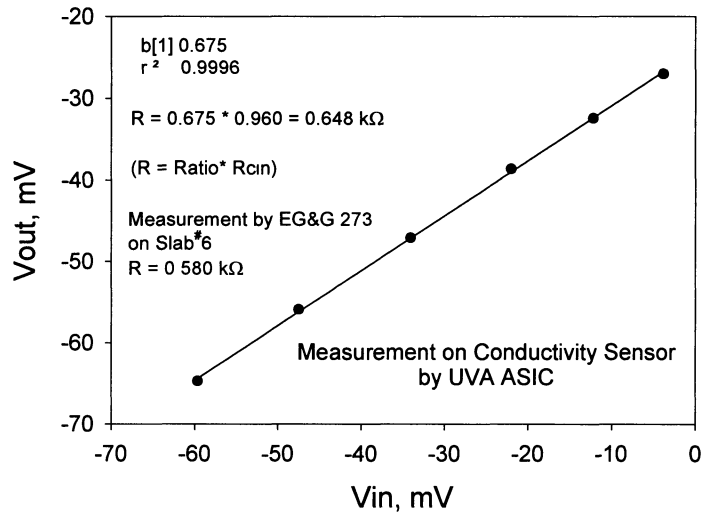


Figure 16. Linear behavior of 4-pin, Au conductivity sensor and μ galvanostat for water-saturated concrete.

The conductivity sensing subsystem was also tested with a concrete block previously made and saturated with water. As shown in Figure 16, a highly linear V_{in} - V_{out} relation in the constant current step scan was found, demonstrating the functionality of the μ Gstat/sensor combination on the ASIC. A resistance value of 0.684 k Ω was measured by the ASIC, compared with 0.580 k Ω measured by a commercial potentiostat (EG&G Model 273). These data were calibrated to a resistivity of around 4 k Ω -cm, based on calibration curves for the sensor. This value was in agreement with data for water-saturated concrete measured by Williams.¹⁶

Measurements of chloride ion concentration were also successful but were very sensitive to the presence of external noise, including that generated by the movement of any nearby object. An investigation of this phenomenon, likely due to the high impedance of the Ag/AgCl interface, is underway as are ways to ameliorate the problem. Nonetheless, the measurements showed that the microinstrument was capable of resolving chloride concentrations as low as 1 mmol/l, which is below the critical chloride concentration for corrosion in concrete.

In summary, the system performs well, but we continue to analyze noise and interference phenomena. When the RF transceiver double-sided surface-mount board is fully implemented and tested, we will construct the field-deployable microinstrument composed of both boards and associated sensors.

A photograph of the packaging for first generation, field-deployable microinstrument is shown in Figure 17. The sensor package includes a piece of reinforcing steel as a working electrode, a platinized niobium mesh counter electrode, a Ag/AgCl wire reference electrode, and a gold four-pin conductivity sensor. The wire bundle leading out of the package allows assessment of the performance of individual electronic subassemblies during the testing phase. The sensor package is mounted on top of a 8 x 4 x 3 cm high impact plastic box that contains the surface mount boards as shown in Figure 17. Future generations of the microinstrument will focus on increasing the level of integration to further reduce the size of the system.

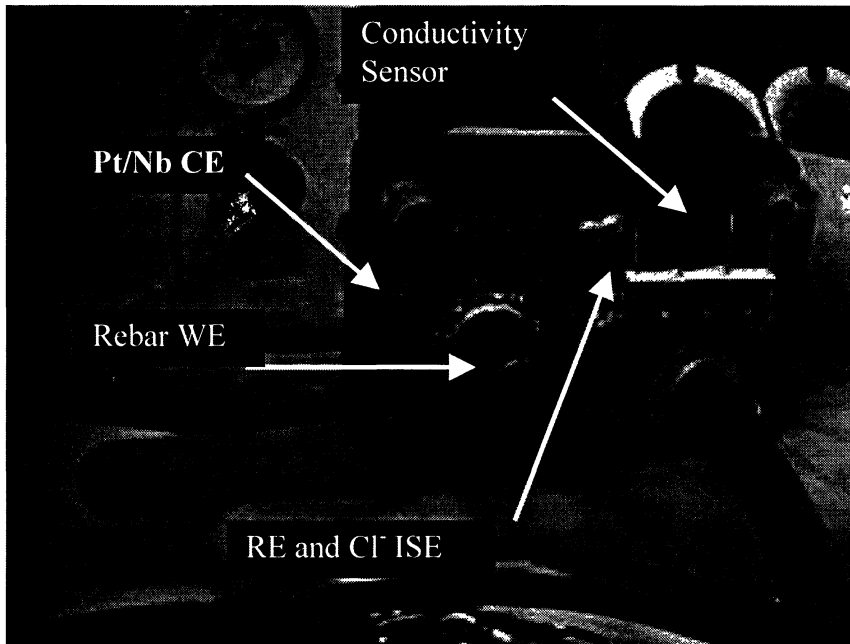


Figure 17. Photograph of sensor arrangement. This top fits onto the box that will contain the surface mount boards.

Sensor Performance in the Concrete Test Structures

Chloride Sensor

Figure 18 shows the potential of two Ag/AgCl electrodes acting as Cl⁻ sensors during electrochemical Cl⁻ driving into test structure 1. It is seen that the Ag/AgCl electrodes responded well to both Cl⁻ intrusion and extraction. Applying the calibration in sat. Ca(OH)₂ solutions of different Cl⁻ content at the beginning the chloride concentration inside the pore water was less than 0.0023 mol/l. Electrochemical chloride driving increased this concentration up to 0.28 mol/l, and electrochemical chloride removal decreased it again by more than a factor of 10. Though these data cannot be easily converted into weight percent chloride in concrete for this test structure, they provide information on the chloride concentration changes.

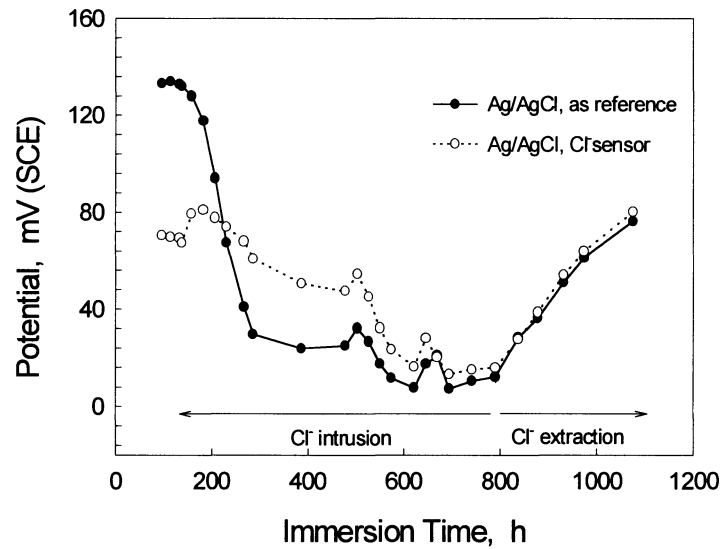


Figure 18. Potential changes of Ag/AgCl electrodes in test structure 1, measured versus a commercial calomel electrode (SCE) immersed in the solution. Decreasing potential indicates increasing chloride ion concentration.

During the chloride intrusion process in test structure 2, a large crack developed on the concrete surface, possibly due to a high pressure of oxygen gas generated at the Ti mesh within the concrete. Because of this crack, the Cl⁻ driving testing was terminated. During the testing, the potentials of some Ag/AgCl electrodes dropped, which might be attributed to either Cl⁻ ingress or electrode failure.

One of the problems during the experiments on the first two slabs was the formation of gases and acid within the concrete at the Ti electrode, potentially damaging the concrete. For the third test structure, the two-chamber system shown in Figure 8 was used to avoid the damage.

The Ag/AgCl electrodes were used as reference electrodes in the corrosion sensors and as chloride sensors when compared to a true reference electrode (in these experiments a SCE). The potential across the electrode/solution interface of an Ag/AgCl electrode is determined by the local Cl⁻ concentration. Concrete represents a very different electrolyte relative to aqueous solution in which this type of electrode is normally employed. Therefore, it was necessary to study the stability and responses of these electrodes in concrete under the conditions of (1) no Cl⁻ in concrete, (2) different Cl⁻ concentration added in the concrete mixes, and (3) dynamic changes of Cl⁻ as a result of electrochemically Cl⁻ driving.

The calibration (Figure 19) made from seven slabs with different Cl⁻ levels showed that the Ag/AgCl electrodes were sensitive to Cl⁻ concentrations as low as 0.01% of the concrete weight. As this value is below the threshold Cl⁻ concentration to induce corrosion of rebar in concrete, the electrodes would be useful for indicating a change in Cl⁻ content sufficient for corrosion initiation.

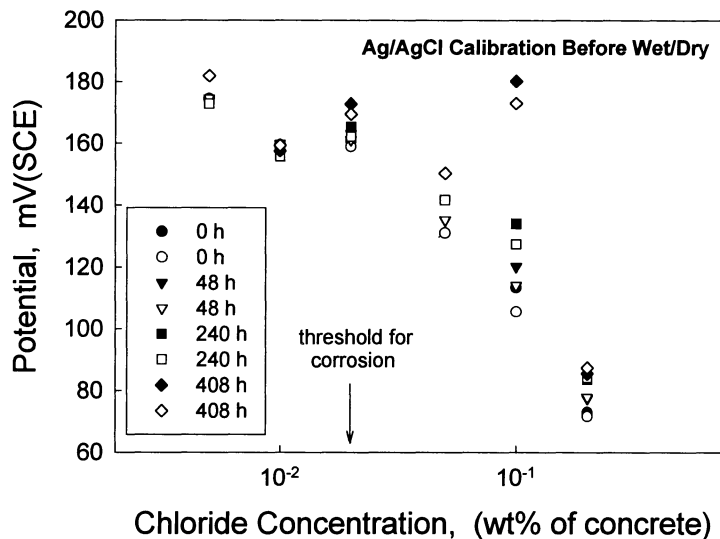


Figure 19. Calibration data for Ag/AgCl sensors in slabs of test structure 3. In each slab two Ag/AgCl electrodes (open and filled symbols) were embedded. Multiple symbols at each concentration show that some sensors had potentials, which increased with time.

The potentials of all the Cl^- sensors moved in the positive direction during the first 400 h of immersion in a saturated $\text{Ca}(\text{OH})_2$ solution. Upon re-immersion in saturated $\text{Ca}(\text{OH})_2$ after drying, all the potentials dropped to different extents, showing the effect of moisture content in concrete. As the concrete slabs regained their moisture contents, the potentials of Ag/AgCl electrodes recovered quickly and eventually surpassed their original values before drying and finally leveled off. Possible explanations for the potential increases include (1) a change in the surface layer (Ag/AgCl) of the electrodes by long-term contact with alkaline environments, or (2) a change in concrete by the wet/dry cycling (see also change in polarization resistance, Figure 24).

Although the potentials of Ag/AgCl increased in the wet/dry cycle, the electrodes in slab 3 demonstrated very good responses to the Cl^- changes in the Cl^- driving testing (Figure 20) with the maximum Cl^- concentrations reached about 0.5%, according to the calibration as shown in Figure 19. This is far above the threshold concentration for the onset of corrosion. After about 1000 additional hours of electrochemical chloride removal at 10 mA (not shown in Figure 20), the potential of the Ag/AgCl electrode had risen to approximately +160 mV (SCE), indicating the presence of a chloride concentration comparable to that present initially.

Some of the Ag/AgCl electrodes failed to function at the beginning of concrete testing, and some failed during the testing, exhibiting sudden potential drops. The electrode in the slab baked at 105 C failed after the slab was re-immersed in the solution, whereas the Ag/AgCl in the slab baked at 60 C is still functioning. The reason(s) for the electrode failures need further investigation for long-term embedding of these Cl^- sensors in concrete.

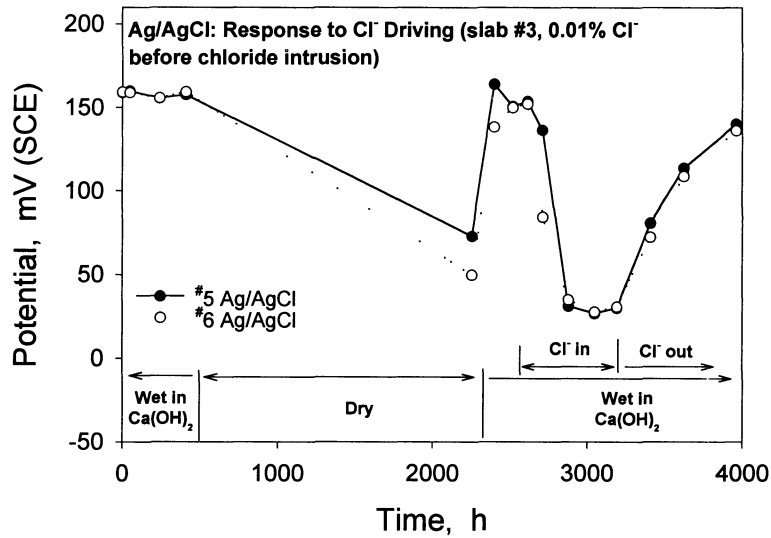


Figure 20. Response of Ag/AgCl electrode to intrusion and removal of chloride.

Corrosion Sensor

Figure 21 shows the potential changes experienced by corrosion sensors and rebar in the test structure 1 during immersion, Cl^- intrusion, and Cl^- extraction. It is seen that the potentials of both corrosion sensors and rebar changed dramatically after about 400 h of electrochemical Cl^- intrusion. The potentials were found to change from about -200 mV in passive state of iron and rebar to a level of about -600 mV, indicating the breakdown of passive film on iron and rebar surfaces by Cl^- and the onset of corrosion. This result was correlated with significant decreases in the polarization resistances of corrosion sensors and rebar (Figure 22).

The polarization resistance of rebar decreased from $\sim 10^3$ to ~ 1 $\text{k}\Omega\text{-cm}^2$, corresponding to a change in corrosion rate from 2×10^{-5} $\mu\text{A}/\text{cm}^2$ to 2×10^{-2} $\mu\text{A}/\text{cm}^2$ after Cl^- intrusion. The polarization resistance values of the two iron corrosion sensors were 175 and 25 $\text{k}\Omega\text{-cm}^2$ measured by the commercial system and commercial OPAMP chip, respectively. The differences in polarization resistance may result from the difference of corrosion resistance between rebar and pure iron or from the heterogeneity in concrete. When the polarity of applied current for chloride driving was reversed and the Cl^- extraction process from concrete started, a further sharp decrease in potential to ~ -900 mV was found for one of the iron corrosion sensors (measured by OPAMP chips) and the rebar (measured with EG&G 273) with the former soon returning to potentials near that observed before Cl^- intrusion.

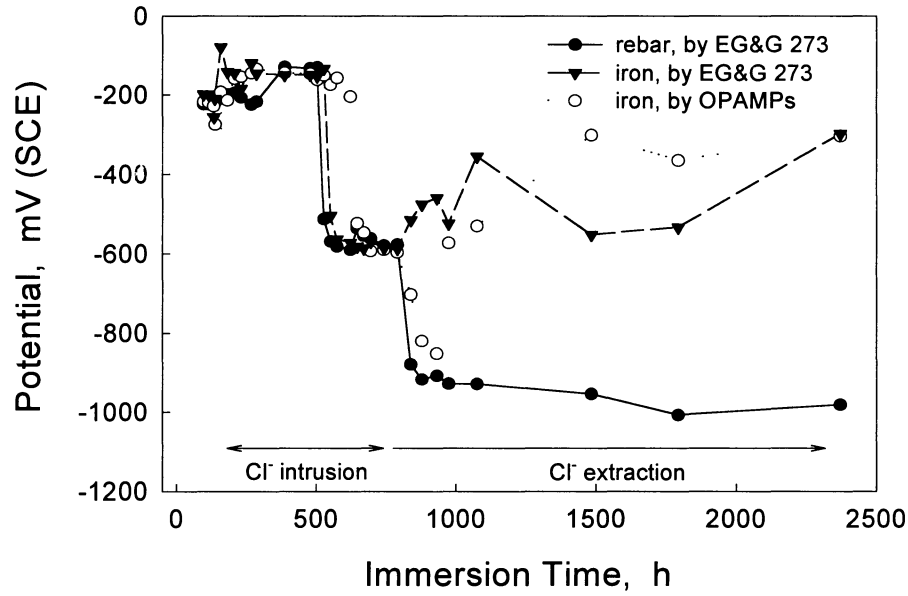


Figure 21. Changes in the open circuit potentials of the corrosion sensors (pure iron) and the rebar sample in test structure 1.

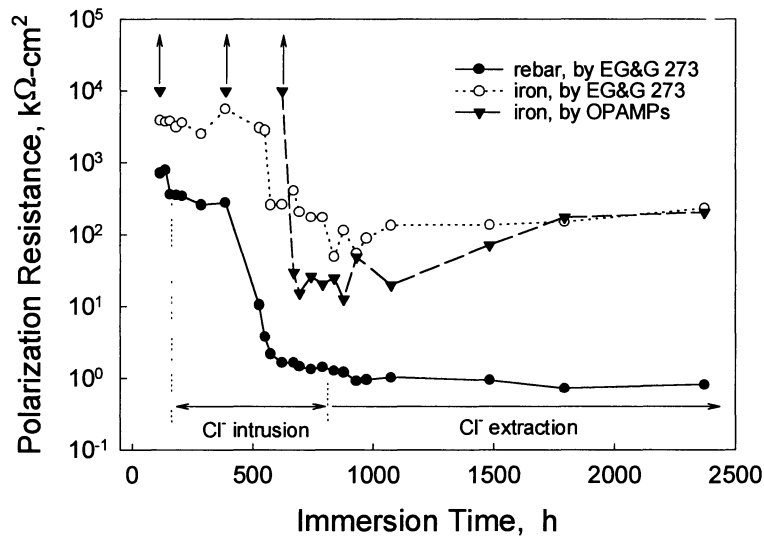


Figure 22. Polarization resistance of the corrosion sensors (pure iron) and the rebar sample in test structure 1.

The changes of potentials in the initial period of Cl^- extraction process indicated the possibility that H^+ , which was generated at the anodic Ti mesh as a result of oxidation of OH^- , was affecting the rebar sample. Under the electrical field for Cl^- extraction from concrete, H^+ ions would migrate into concrete, causing a pH drop inside concrete and further decreases in the potential of the rebar and pure iron. The pH change during Cl^- intrusion is caused by the consumption of OH^- ions at the anodic Ti mesh inside concrete. It occurs at a more distant place from the position of the rebar and corrosion sensor (see Figure 5, 25 mm concrete instead of 10

mm). Therefore, its effect should be less significant. Because the external testing solution became significantly acidic after Cl^- extraction, $\text{Ca}(\text{OH})_2$ was added to saturation to eliminate the effect of H^+ migration by raising the solution pH. It was found that the potentials of both corrosion sensors gradually increased to about -300 mV. High polarization resistance in Figure 22 indicates the repassivation of pure iron. However, the potential of rebar was still very negative and its corrosion rate remained basically unchanged after Cl^- extraction.

The measurements of polarization resistance with the commercial LMC6034 OPAMP chip in connection with electrochemical intrusion and extraction of chloride demonstrated that the use of the $\mu\text{Pstat}/\mu\text{ZRA}$ combination is feasible for the detection of the onset of iron corrosion in concrete. The electrochemical Cl^- driving technique applied in this work proved to be a very effective accelerated testing method in inducing corrosion of iron and rebar in concrete within several weeks, which are significantly less than the time needed for ponding.

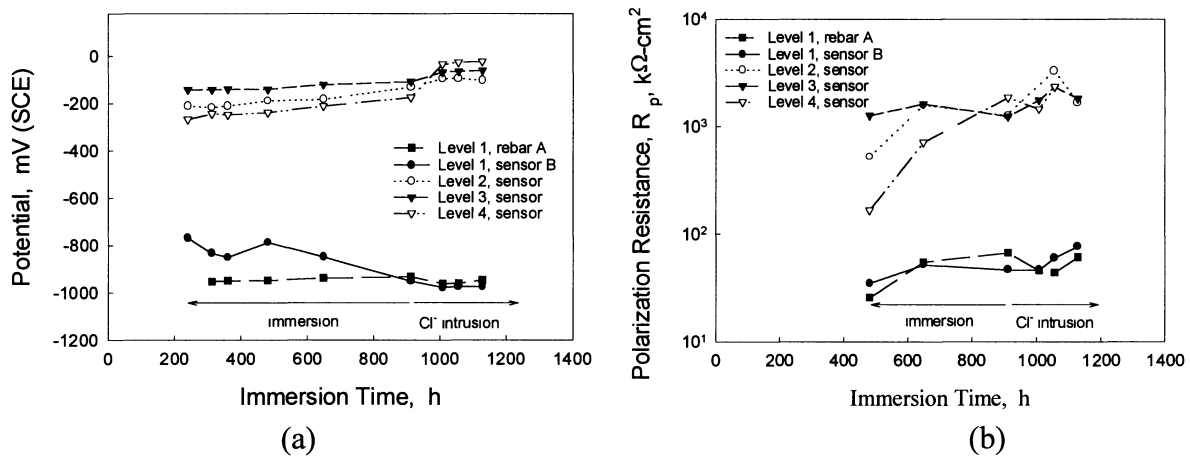


Figure 23. (a) Open circuit potentials and (b) polarization resistances of corrosion sensors at the four levels in test structure 2.

The second test structure was immersed in deionized water to allow the establishment of a steady state. After several days of immersion in deionized water, corrosion was found to have initiated on the rebar specimen and the two corrosion sensors at the first level (see Figure 6) although no chloride had been added to the slab mixture and no chloride was in solution. Although the explanation for the corrosion before Cl^- intrusion remains unclear, the onset of corrosion at the first level allowed a quick evaluation of the $\mu\text{Pstat}/\mu\text{ZRA}$ and μGstat comprised of the first VLSI design of OPAMP chips. Figure 23a shows the potentials of rebar specimens and corrosion sensors at the different levels. At the first level, the potentials of rebar A and sensor B were in the active dissolution region of rebar after 1000 h of immersion. Polarization resistance measurements in Figure 23b indicated that corrosion of rebar happened at this level. The corrosion rates measured by $\mu\text{Pstat}/\mu\text{ZRA}$ on corrosion sensors and by the commercial measuring system on rebar specimens were nearly the same, with the corresponding corrosion rates about 50 times less than that of rebar in the presence of Cl^- (Figure 22). Figure 23 also shows that the $\mu\text{Pstat}/\mu\text{ZRA}$ of the first VLSI design even has the ability to detect the extremely

small dissolution current of rebar at its passive state, as compared with the $\mu\text{Pstat}/\mu\text{ZRA}$ by the commercial OPAMP chips.

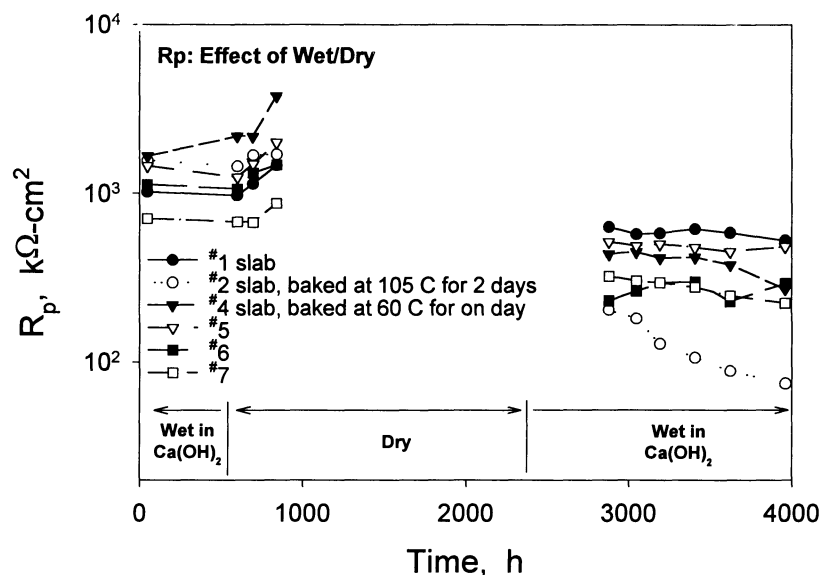


Figure 24. Polarization resistance values for sensors in slabs of test structure 3 during wet/dry cycling.

For test structure 3 (Figure 7, Table 1), after the 400 h of soaking in $\text{Ca}(\text{OH})_2$, wet/dry testing of the slabs was initiated. Before drying started, all the corrosion sensors were in passive states (high R_p and E_{corr} values). The R_p values (Figure 24) at this stage ($\sim 1 \text{ M}\Omega\text{-cm}^2$) were very close to those of passivated corrosion sensors in the second concrete slab, which was in a state of constant water saturation. After drying in air and re-immersion in saturated $\text{Ca}(\text{OH})_2$ solution, significant decreases in R_p values were observed for all the slabs.

It is interesting to note that slab 2, which was baked at 105 C and had some large cracks across its surface, underwent the largest changes in E_{corr} and R_p . After drying and re-immersion, both E_{corr} (Figure 25) and R_p dropped dramatically but not to a level that was considered a completely active dissolution state. A similar behavior was found for slab 4, which was baked at 60 C for one day. Slabs 2 and 4 had very low concentrations of Cl^- , so the origin of the move toward the activation of the corrosion sensor is not clear.

The inclusion of different amounts of NaCl in the mixes for the different slabs led to interesting results. The corrosion sensors in slabs 1, 4, 5, 6, and 7 were initially passivated, showing high E_{corr} ($> -100 \text{ mV vs. SCE}$) and high R_p ($\sim 500 \text{ k}\Omega\text{-cm}^2$), although these slabs contained different levels of Cl^- (0 - 0.2% of the concrete weight). The critical Cl^- concentration for rebar corrosion has been reported to be 0.02 wt.%. The failure to induce corrosion on the corrosion sensors might have been the result of any of a number of factors: (1) bonding of the Cl^- added to the cement may have resulted in lower effective Cl^- concentrations, (2) the immersion time may have been shorter than required for activation, or (3) the Cl^- may have been unevenly distributed. A close examination of the measured R_p values revealed that Cl^- did have an influence on R_p . For the slabs that were dried in air at room temperature, the higher the chloride

content in the slabs, the lower the rewetted polarization resistance. Drying of slabs in the moisture chamber caused increases in R_p . This result was expected.

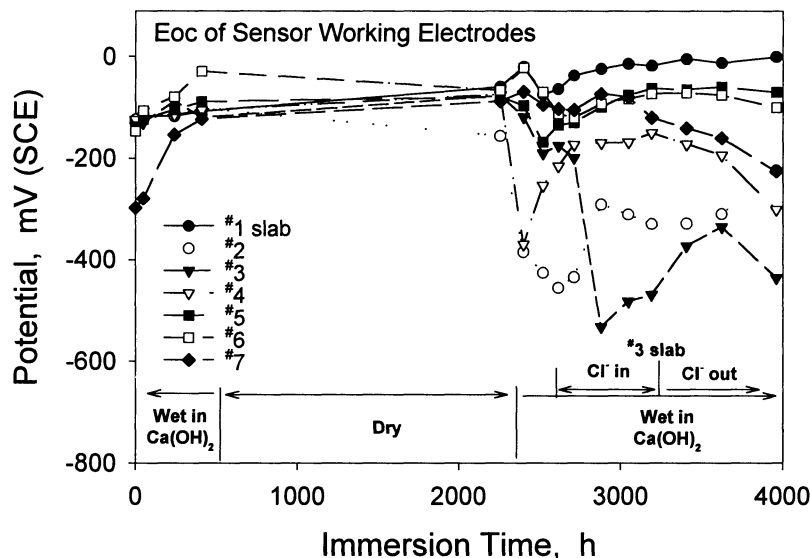


Figure 25. Corrosion potentials of sensors in test structure 3.

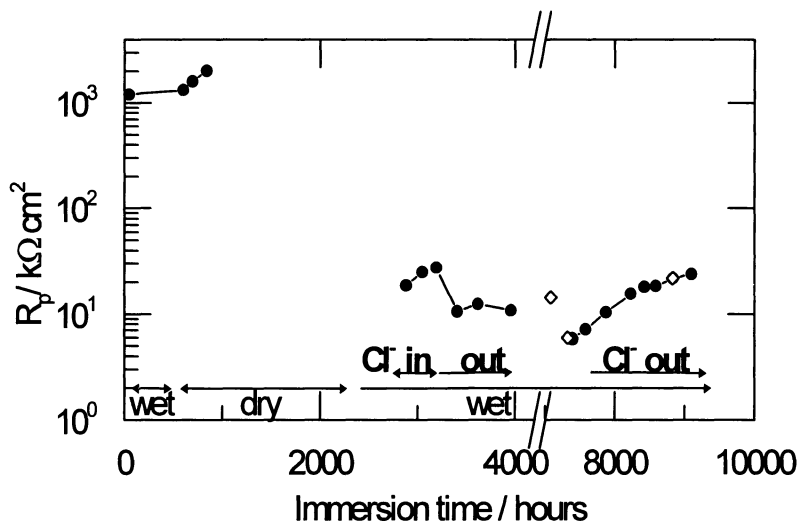


Figure 26. Polarization resistance change of slab 3 upon electrochemical chloride driving.

For slab 3, Cl^- driving at 10 mA for about 500 h (comp. Figure 20) induced corrosion on the corrosion sensor as shown in Figure 25. The initiation of corrosion was indicated by both a drop in E_{corr} from -100 to -500 mV vs. SCE and a decrease in R_p from $>1 \text{ M}\Omega\text{-cm}^2$ to $\sim 18 \text{ k}\Omega\text{-cm}^2$. When the polarity of the applied current was reversed and the Cl^- driving-out started, the E_{corr} responded with an increase toward the passive state, but R_p decreased further and then increased very slowly, as in the case of the test structure 1. As of the date of this report, 2000 additional

hours of chloride extraction at 10 mA has resulted in a corrosion potential of -0.1 V (SCE), indicating repassivation of the steel, but the R_p value remains low ($24 \text{ k}\Omega\text{-cm}^2$), indicating inhibited, but continued corrosion (Figure 26).

Conductivity Sensor

The conductivity measurements failed in test structure 1. The sensor may have malfunctioned because of a failure of the operational amplifiers or the electrode connectors.

The resistivity sensors embedded in the slabs of test structure 2 (Figure 6) and test structure 3 (Figure 7) worked well, as shown in Figure 27. When saturated with water, the measured resistances ranged from 300 to 500 Ω , corresponding to the resistivity values of 1870 to 3307 $\Omega \text{ cm}$, in agreement with the data in previous work.¹⁶ Drying the slabs in a humidity chamber at 90, 70, 50, and 30% RH for 4 days, respectively, resulted in a limited increase (about 50%) in the concrete resistance. Drying in air (40 to 50%RH) for about 1,500 h increased the resistivity up to 11,250 to 15,600 $\Omega\text{-cm}$. Mild heating at 60 C for one day (slab #4) led to a resistivity as high as 16,400 $\Omega\text{-cm}$. More aggressive drying of slab 2 (105 C for 2 days) caused the resistance to rise to a level that the electrochemical measurements for resistance were not possible. As shown for slab 3, chloride intrusion/extraction seemed to cause large resistivity fluctuation (2000 to 7000 $\Omega\text{-cm}$). The mechanism behind this phenomenon is unknown at this time.

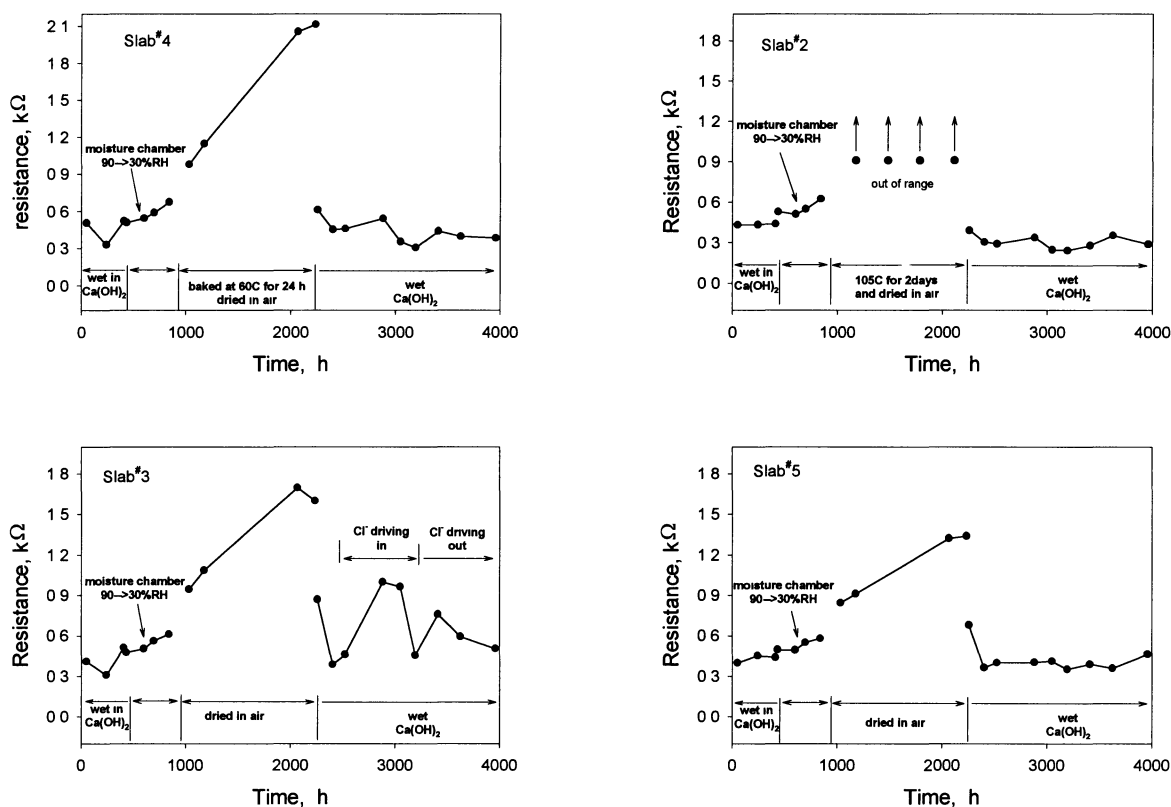


Figure 27. Resistance vs. time plots for several of the slabs from test structure 3. Different drying practices led to different levels of resistance, as expected. Electrochemical chloride addition and removal led to significant fluctuations in resistivity.

pH Sensor

The pH measurements failed in test structure 1. The potential changes recorded during electrochemical chloride intrusion and removal process gave unreasonable pH values for concrete. The failure of W/WO₃ electrodes in monitoring pH change may lie in the nature of the electrode. Although good pH responses were found for W/WO₃ electrodes under some conditions,^{17,18} their sensitivity to Ca²⁺,¹⁹ which is the major component of cement, poses a major problem for the application in concrete. It was decided that pH measurements in concrete were not as important as moving the project forward to the field testing stage as quickly as possible, so pH measurement schemes were abandoned.

Embeddable Reference Electrodes for Concrete

Based upon the work of Pawlick,⁸ Ag/Pb and Au/Cu galvanic couple reference electrodes were embedded in the first test structure. These were selected based upon their stability in saturated Ca(OH)₂ solutions. Unfortunately, neither of these electrodes showed reproducible, stable behavior in concrete (Figure 28). The electrodes appeared to be stable until chloride was electrochemically driven into the concrete, at which point a marked change occurred. Whether this change was due to the chloride ingress or a local change in pH as discussed was not clear.

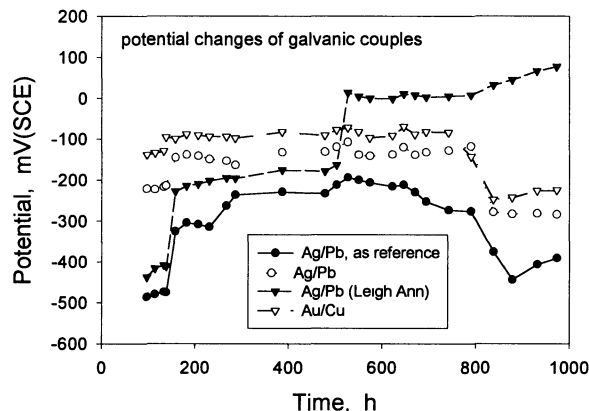


Figure 28. Potential vs. time for Ag/Pb and Au/Cu galvanic couple reference electrodes in test structure 1.

In test structure 3, a range of reference electrodes were embedded in each block, allowing the effects of chloride content, wet/dry cycling, and electrochemical chloride movement to be assessed. A range of electrodes was studied, as detailed in Table 1. Unfortunately, most of the electrodes had unstable potentials, as shown in Figure 29. Most types of reference electrode had either large potential fluctuations (graphite, C-fiber, Mo, Sn, NiOOH) or active-passive transitions (Co, Ni) during the concrete testing. Consider that a potential change of only 60 mV in the potential of the reference electrode leads to an order of magnitude change in the estimate of the chloride concentration measured by the chloride sensor (versus that reference electrode).

Pb single electrode and W/Ni couple seemed to be the most suitable candidates for the embeddable reference electrodes in concrete among the electrodes studied. The question, which electrode is suitable as a long-term stable, embeddable reference electrode must be answered by additional studies.

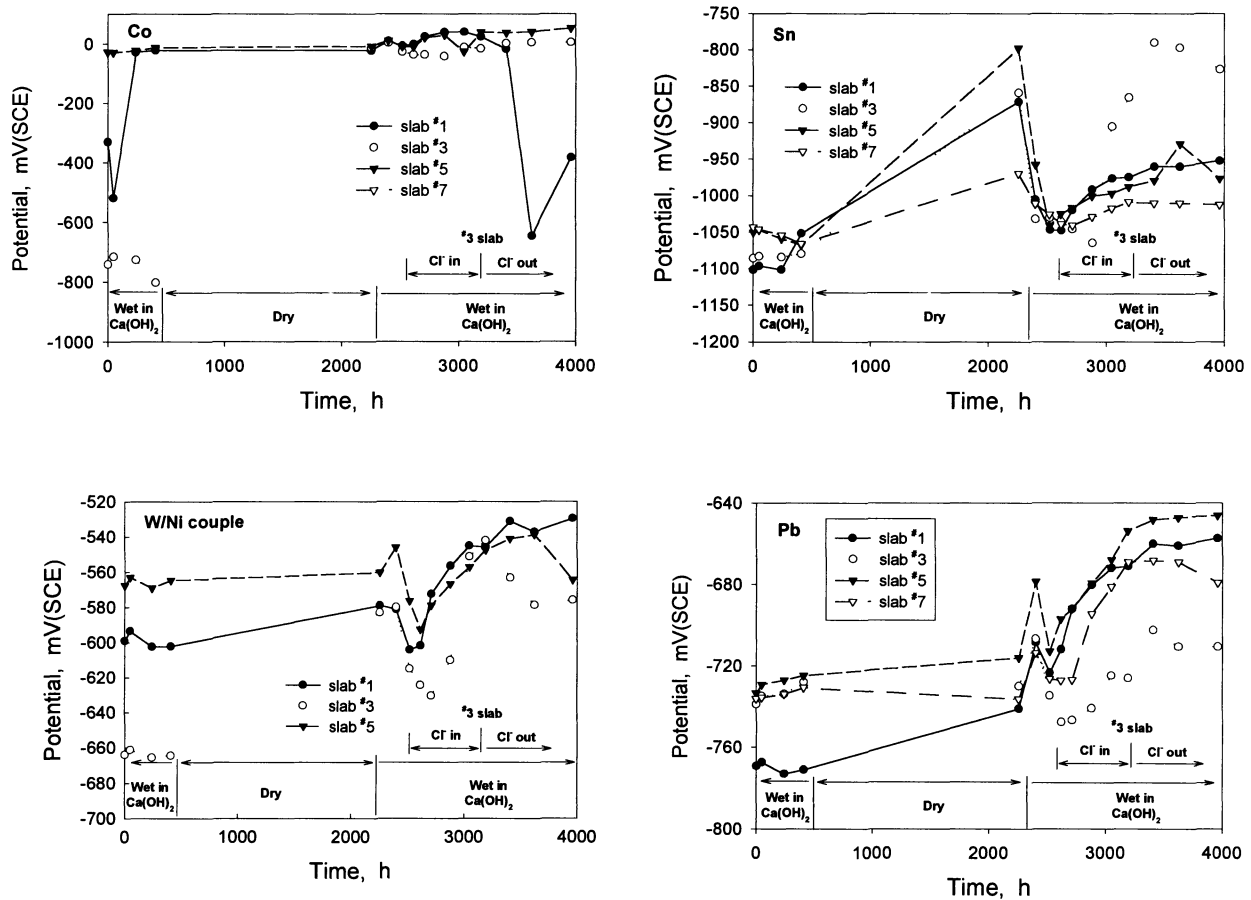


Figure 29. Potential vs. time data for four of the reference electrode types studied in the test structure 3 slabs. Only the W/Ni and Pb electrodes showed reasonable stability with time, chloride content, and drying. Note the different scales on each plot.

Coatings for Encapsulation

The concrete slabs of test structure 3 also allowed testing of different encapsulation materials. Such materials will be needed for sealing of the device (with exception of the sensors) to prevent corrosion of the electronics. As outlined in Table 1, steel sheets coated with four different commercial products were embedded. Electrochemical impedance spectroscopy was used to monitor the protectiveness of the coatings. The magnitude of the impedance at 100 mHz was used as a figure of merit for the protectiveness. As Figure 30 shows, the E-bond and 680/705 coating systems provided the best performance. These studies are ongoing.

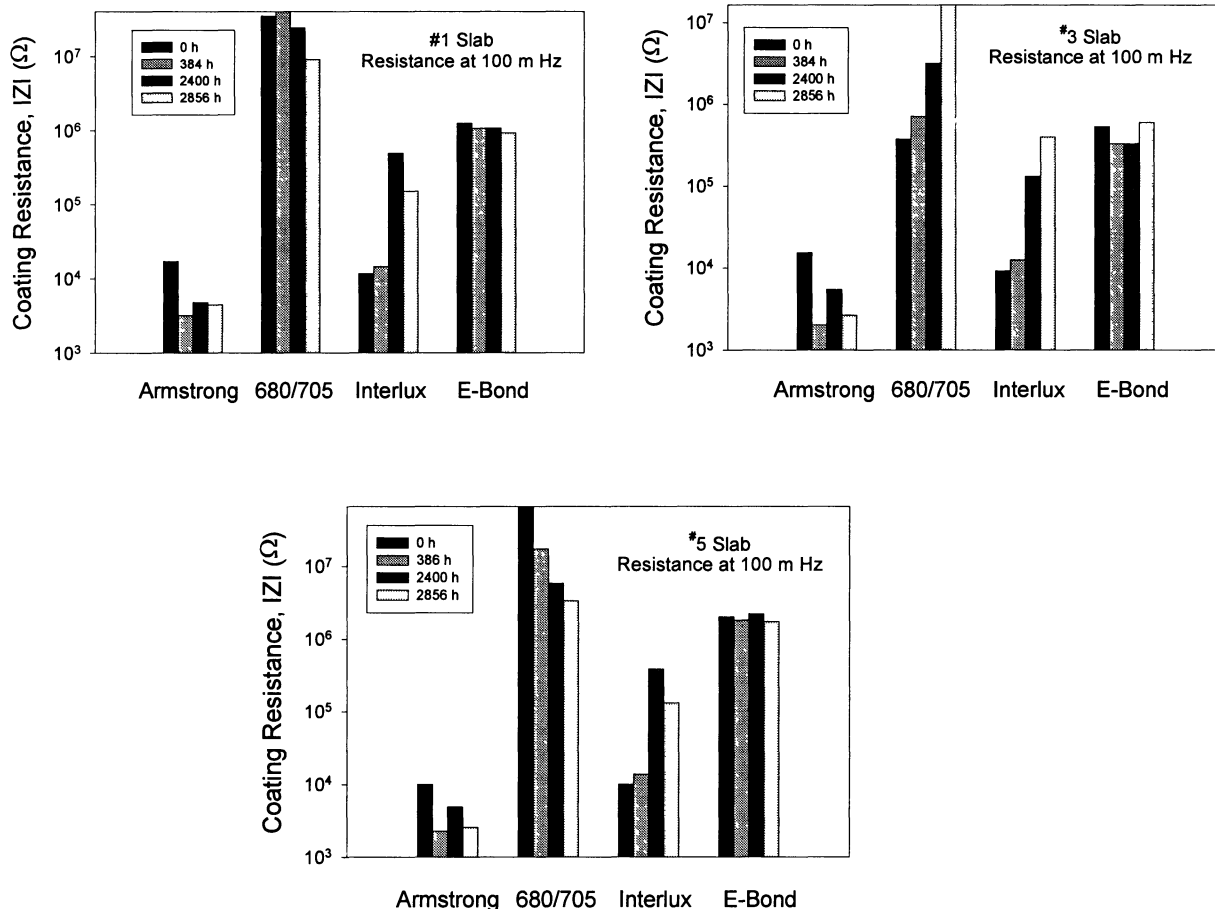


Figure 30. Low-frequency magnitude of the impedance of coated steel for four different coating systems as a function of time and chloride content (chloride content increases with slab number).

SUMMARY

A laboratory prototype of a microinstrument for monitoring of corrosivity in concrete was developed that contains sensors for corrosion potential and polarization resistance of rebar material, concrete conductivity, chloride concentration, temperature, and a reference electrode. This instrument will be completely embedded inside of concrete structures without any wires leading from the instrument to the outside of the concrete.

The electronic circuits necessary to perform all measurements were designed based on an application specific integrated circuit (ASIC) as the main component. Several generations of the electronics were implemented via MOSIS and were successfully tested with dummy cells, corroding steel samples in solutions, and sensors embedded in concrete.

The present system is integrated onto two double-sided, surface mount boards. One board contains the ASIC, a microprocessor, control circuitry, and connections to the external corrosivity sensors; the other board contains communication circuitry to allow wireless communication with the microinstrument via RF transmission.

The corrosion sensor contains rebar material as a working electrode and a platinized Nb-mesh as counter electrode. For the measurement of the corrosion potential, a long-term stable reference electrode is needed. For the measurement of the polarization resistance, this is not required. The microinstrument is able to measure the polarization resistances of steel whether the rebar is in active or passive state. The corrosion sensor works well.

The conductivity sensor made from four Au-wires is based on a modified Wenner four-pin method and works very well with the microinstrument.

The chloride sensor (Ag/AgCl) responds very well to the concentration changes during electrochemical chloride intrusion and extraction and is sensitive to chloride concentrations lower than the corrosion threshold for concrete. However, some of the observed changes during wet/dry cycling are not completely understood and need further investigation.

Several candidates for small, embeddable reference electrodes were tested. Ni/W and Pb seem to be promising candidates. However, none of the electrodes worked perfectly. This might be related to coating failure. More tests with a better coating are necessary to solve this problem. Good coating materials have been found by impedance measurements on steel panels, which were treated with the different coatings prior to embedding them in concrete.

The costs for a single microinstrument of the present design can be estimated to be about \$ 2000, which includes the commercial electronics (A/D, D/A/, processor, RF communication). All these costs can be expected to come down significantly upon mass production, by a factor of 4.

FUTURE RESEARCH AND IMPLEMENTATION

Upcoming experiments will focus on the development of a field-deployable prototype of the microinstrument. This prototype will include the whole electronics and the external sensors, packaged as shown in Figure 17. A series of tests will be done on the final microinstrument to monitor all aspects of the working electronics. In particular, we will test all the command sequences, data collection, and data transmission functions. The first series of test will use dummy cells (resistor/capacitor combinations) as well as lab scale corrosion cells (i.e., steel in $\text{Ca}(\text{OH})_2$ with and without chloride) with hard-wire connections for communications and control. In this way, all the electronics and sensors can be tested independent of the RF communications board. We will also measure and evaluate the system power consumption with the RF transceiver functionality. The system will be tested then under the same conditions but using the wireless RF transmit and receive functions. These tests will focus on bit errors, noise immunity, and signal interference phenomena as a function of the distance between the microinstrument and the remote receiver. We will also evaluate the microinstrument power consumption under full-autonomous, wireless operation.

Upon completion of these tests and after any required modifications are made, the prototype will be ready to test in the field in cooperation with VTRC and FHWA. Simultaneously with field testing, laboratory testing will continue, focusing on packaging issues

(i.e., case materials, sealants), electronic and system reliability issues, and development of the hardware and software necessary for remote control and data analysis. In addition, several options regarding power will be investigated, including commercially available remote RF power systems and the use of galvanic couples as a reference electrode in the concrete.

We are currently preparing to transfer the technology to two small U.S. companies who have expressed interest in further development, including manufacture.

REFERENCES

1. C. M. Hansson, B. Sørensen, The Threshold concentration of Chloride in Concrete for the Initiation of Reinforcement Corrosion, *Corrosion Rates of Steel in Concrete*, N. S. Berke, V. Chaker, D. Whiting, STP 1065: 3-16, American Society for Testing and Materials, Philadelphia (1990).
2. N. Berke, in *Corrosion Tests and Standards*, R. Baboian, p. 331 Amer. Soc. For Testing and Materials, Philadelphia (1995).
3. J. M. Gaidis, A. M. Rosenberg., I. Saleh, Improved Test Methods for Determining Corrosion Inhibition by Calcium Nitrite in Concrete, *Corrosion of Reinforcing Steel in Concrete*, J. M. Gaidis, D. E. Tonini, STP 713: 64-74, American Society for Testing and Materials, Philadelphia (1980).
4. K. Matsuoka, H. Kihira, S. Ito, T. Murata, Corrosion Monitoring for Reinforcing Bars in Concrete, *Corrosion Rates of Steel in Concrete*, N. S. Berke, V. Chaker, D. Whiting, STP 1065: 103-117, American Society for Testing and Materials, Philadelphia (1990).
5. K. Videm, R. Myrdal, Electrochemical Behavior of Steel in Concrete and Evaluation of the Corrosion Rate, *Corrosion*, 53 734 (1997).
6. J. P. Broomfield, Field Measurement of the Corrosion Rate of Steel in Concrete Using a Microprocessor Controlled Unit with a Monitored Guard Ring for Signal Confinement, *Techniques to Assess the Corrosion Activity of Steel Reinforced Concrete Structures*, N. S. Berke, E. Escalante, C. K. Nmai, D. Whiting, STP 1276: 91-106 American Society for Testing and Materials, Philadelphia (1996).
7. W. Blanke, Mixed-Signal and Sensor Components for the Design of Integrated Circuit Microinstruments, M.S. Thesis, Department of Electrical Engineering, University of Virginia, Charlottesville (May, 1996).
8. L. A. Pawlick, The Development of Embeddable Galvanic Couple Reference Electrodes for Concrete, M.S. Thesis, Department of Materials Science and Engineering, University of Virginia, Charlottesville (May, 1997).

9. ASTM Standard Method for Field Measurement of Soil Resistivity Using the Wenner Four-Electrode Method (G 57-78), Amer. Soc. for Testing and Materials, Philadelphia (1987).
10. D. J. G. Ives, Oxide, Oxygen, and Sulfide Electrodes, *Reference Electrodes*, D. J. G. Ives and G. J. Janz, 322-392, Academic Press, New York (1961).
11. S. Gottesfeld and J. D. E. McIntyre, Electrochromism in Anodic Oxide Films II. pH Effects on Corrosion Stability and the mechanism of coloration and bleaching, *J. Electrochem. Soc.*, 126: 742 (1979).
12. S. Dexter, Marine Corrosion: Seawater, *Corrosion*, ASM Handbook, Vol. 13: 898 American Society for Metals, Metals Park, Ohio (1987).
13. M. G. Fontana, N. D. Greene, *Corrosion Engineering*, McGraw-Hill, New York (1978) p. 269.
14. C. M. Hansson, B. Sørensen, The Threshold concentration of Chloride in Concrete for the Initiation of Reinforcement Corrosion, *Corrosion Rates of Steel in Concrete*, N. S. Berke, V. Chaker, D. Whiting, STP 1065: 3-16, American Society for Testing and Materials, Philadelphia (1990).
15. N. S. Berke, D. F. Shen, K. M. Sundberg, Comparison of the Polarization Resistance technique to the Macrocell Corrosion Technique, *Corrosion Rates of Steel in Concrete*, N. S. Berke, V. Chaker, D. Whiting, STP 1065: 38-51, American Society for Testing and Materials, Philadelphia (1990).
16. A. Williams, Determination of safe cathodic protection limit for prestressed concrete pilings: Electrochemical conditions in pilings subject to cathodic protection, M.S. Thesis, Department of Materials Science and Engineering, University of Virginia, Charlottesville (1995).
17. C. T. Abichandani, S. K. K. Jatkar, *J. Indian Inst. Sci.*, 21A, p. 345 (1939).
18. H. Brintzinger, B. Rost, *Z. Anal. Chem.*, 120, p. 161 (1940).
19. P. C. Caldwell, *J. Physiol.*, 126, p. 169 (1954).